Report Prepared by:

Andrea N. Sánchez
Alberto A. Sagüés

FINAL REPORT

MODELING REINFORCED CONCRETE DURABILITY

Contract No. BDK84 977-09
Final Report to Florida Department of Transportation

A. A. Sagüés
Principal Investigator
Department of Civil and Environmental Engineering

Tampa, FL 33620
June 2014

DISCLAIMER

The opinions, findings, and conclusions expressed in this publication are those of the authors and not necessarily those of the State of Florida Department of Transportation.

Universal Conversion Table

SI* (MODERN METRIC) CONVERSION FACTORS

APPROXIMATE CONVERSIONS TO SI UNITS

Symbol	When You Know	Multiply By	To Find	Symbol
		LENGTH		
in	inches	25.4	millimeters	mm
ft	feet	0.305	meters	m
yd	yards	0.914	meters	m
mi	miles	1.61	kilometers	km
		AREA		
in^2	square inches	645.2	square millimeters	mm^2
ft^2	square feet	0.093	square meters	m^2
yd^2	square yard	0.836	square meters	m^2
ac	acres	0.405	hectares	ha
mi^2	square miles	2.59	square kilometers	km^2
		VOLUME		
fl oz	fluid ounces	29.57	milliliters	mL
gal	gallons	3.785	liters	L
ft^3	cubic feet	0.028	cubic meters	m^3
yd^3	cubic yards	0.765	cubic meters	m^3
		NOTE: volumes greater than 1000 L shall be shown in m^3		
		MASS		
oz	ounces	28.35	grams	g
lb	pounds	0.454	kilograms	kg
T	short tons (2000 lb)	0.907	megagrams (or "metric ton")	Mg (or "t")
		TEMPERATURE (exact degrees)		
°F	Fahrenheit	5 (F-32)/9 or (F-32)/1.8	Celsius	°C
		ILLUMINATION		
fc	foot-candles	10.76	lux	lx
fl	foot-Lamberts	3.426	$candela/m^2$	cd/m^2
		FORCE and PRESSURE or STRESS		
lbf	poundforce	4.45	newtons	N
lbf/in^2	poundforce per square inch	6.89	kilopascals	kPa

APPROXIMATE CONVERSIONS FROM SI UNITS

Symbol	When You Know	Multiply By	To Find	Symbol
		LENGTH		
mm	millimeters	0.039	inches	in
m	meters	3.28	feet	ft
m	meters	1.09	yards	yd
km	kilometers	0.621	miles	mi
		AREA		
mm^2	square millimeters	0.0016	square inches	in^2
m^2	square meters	10.764	square feet	ft^2
m^2	square meters	1.195	square yards	yd^2
ha	hectares	2.47	acres	ac
km^2	square kilometers	0.386	square miles	mi^2
		VOLUME		
mL	milliliters	0.034	fluid ounces	fl oz
L	liters	0.264	gallons	gal
m^3	cubic meters	35.314	cubic feet	ft^3
m^3	cubic meters	1.307	cubic yards	yd^3
		MASS		
g	grams	0.035	ounces	oz
kg	kilograms	2.202	pounds	lb
Mg (or "t")	megagrams (or "metric ton")	1.103	short tons (2000 lb)	T
		TEMPERATURE (exact degrees)		
°C	Celsius	1.8C+32	Fahrenheit	°F
		ILLUMINATION		
lx	lux	0.0929	foot-candles	fc
cd/m^2	$candela/m^2$	0.2919	foot-Lamberts	fl
		FORCE and PRESSURE or STRESS		
N	newtons	0.225	poundforce	lbf
kPa	kilopascals	0.145	poundforce per square inch	lbf/in^2

*SI is the symbol for the International System of Units. Appropriate rounding should be made to comply with Section 4 of ASTM E380.

TECHNICAL REPORT DOCUMENTATION PAGE

1. Report No.	2. Government Accession No.	3. Recipient's Catalog No.
4. Title and Subtitle **MODELING REINFORCED CONCRETE DURABILITY**		5. Report Date June 2nd, 2014
		6. Performing Organization Code
7. Author(s) A.N. Sánchez and A.A. Sagüés		8. Performing Organization Report No.
9. Performing Organization Name and Address Department of Civil and Environmental Engineering University of South Florida (USF) Tampa, FL 33620		10. Work Unit No. (TRAIS)
		11. Contract or Grant No. BDK84-977-09
12. Sponsoring Agency Name and Address Florida Department of Transportation 605 Suwannee St. MS 30 Tallahassee, Florida 32399 (850)414-4615		13. Type of Report and Period Covered Final Report 01/01/2010 - 06/03/2014
		14. Sponsoring Agency Code

15. Supplementary Notes

16 Abstract: This project developed a next-generation modeling approach for projecting the extent of reinforced concrete corrosion-related damage, customized for new and existing Florida Department of Transportation bridges and suitable for adapting to broader use within the FDOT. The modeling approach incorporates a series of advanced features that include in the first place a probabilistic treatment of the damage prediction calculations with statistical variability in surface concentration, concrete cover, and chloride diffusion coefficient. Additionally, the model incorporates the effect of steel potential on corrosion threshold by the use of a potential-dependent threshold correction function. Additional features are type of rebar material, geometric aggravation effects from rebar presence, and corners and curvature in the concrete surface. The model has also functionality for variability in environmental aggressiveness conditions as a function of elevation above water and for location of structural components in various environments in the same bridge. Experiments were conducted to resolve shortages in potential-dependent threshold data. The results produced improved input parameters for the model calculations that developed the threshold-effect correction function.

17. Key Words	18. Distribution Statement
Reinforced concrete, corrosion, damage, modeling, reinforcing steel, durability, concrete.	No Restriction This report is available to the public through the NTIS, Springfield, VA 22161

19. Security Classif. (of this report)	20. Security Classif. (of this page)	21. No. of Pages	22. Price
Unclassified	Unclassified	73	

ACKNOWLEDGEMENT

The assistance of Ronald Simmons and Cody Owen in specimen autopsy and conducting chloride analysis tests at the FDOT State Materials Office is gratefully acknowledged. The assistance of student participants in the University of South Florida, College of Engineering Research Experience for Undergraduates (Juan Cardenas, Cesar Castañeda, Randy Guillen, Andrew Filippi, William Ruth, and Thuyen Tran) is also acknowledged. The authors are indebted to Mr. Mario Paredes from the FDOT State Materials Office for all his valuable guidance.

EXECUTIVE SUMMARY

Corrosion of steel in concrete is a major limitation of the durability of the Florida Department of Transportation (FDOT) bridges, especially for those in marine service. Accumulation of expansive corrosion products at the steel surface creates tensile stresses in the concrete surrounding the rebar and consequent cracking and spalling of the concrete. Expensive maintenance repair and subsequent corrosion control is then needed.

The FDOT has instituted corrosion prevention practices that include the use of very low permeability concrete and increased concrete cover thickness over the steel. Those practices represent increased initial cost. Thus, accurate projection of the durability gains which may be obtained for a given initial investment is needed. Additionally, it is important to tailor the design to the environmental conditions present at each bridge site and to the specified service life for that bridge. It is also often necessary to obtain a quantitative projection of the remaining corrosion-related service life of a structure for decision making on whether to build a new structure or continue using the existing one. Projections should be sophisticated enough to estimate not only the structure age when substantial damage will appear, but also the rate at which subsequent corrosion damage would develop. The damage projection models used by FDOT at the beginning of this project represented a major improvement over the more qualitative approaches used in the past. However, most of those models have been prepared for and used by specialists only and have tended to address only selected combinations of critical factors without an integrated approach.

This project developed a next-generation modeling approach for projecting the extent of reinforced concrete corrosion-related damage, customized for FDOT bridges and suitable for adapting to broader use within the FDOT. Tasks conducted to achieve the objective included identifying critical features which need to be incorporated for an efficient modeling approach, expansion in information as input to the identified critical features in the previous task, and implementation of that information in a durability projection prototype suitable for development into software matching that used in similar protocols by the State Materials Office.

Identification of critical features showed that incorporation of a potential-dependent threshold (PDT) for corrosion initiation, largely ignored in current predictive models, was necessary to make more realistic model projections. That feature permits accounting for corrosion macrocell coupling between active and passive steel assembly components, avoiding overly conservative long-term damage projections and leading to more efficient design. To incorporate PDT in prediction modeling, experiments were conducted to better characterize the extent of the effect and to obtain more accurate parameters as model inputs. The experiments were conducted with mortar and concrete specimens in conditions more realistic than those available previously. The results confirmed the presence of the effect and provided supporting information to use a value of 550 mV per decade of Cl^- for the cathodic prevention slope $|\beta_{CT}|$, a critical quantitative input for implementation in a practical model.

A mathematical model created in earlier FDOT projects was refined to accurately incorporate PDT and used to conduct a series of comparative calculations with and without that feature, so as to develop a correction factor for calculations performed without PDT. The calculations were conducted with a simulated partially submerged

reinforced concrete column representative of conditions prevalent in aggressive marine bridge service.

The next-generation model created under this project incorporates a series of advanced features responding to the objectives of the project. Those features include a full probabilistic treatment of the damage prediction calculations, with statistical variability in surface concentration, concrete cover and chloride diffusion coefficient, and incorporation of PDT through the correction factor described above. The model allows for the type of rebar material and the detrimental effect of chloride flow obstruction by the rebar and the geometric aggravation that results from the presence of corners and curvature in the concrete surface. Furthermore, in response to the need for another critical feature identified during the initial stages of the project, the model incorporates also functionality to allow for variability in environmental aggressiveness conditions as a function of elevation above water and for location of structural components in various environments within the same bridge. Those features permit specific design for different parts of the bridge, thus avoiding over-specification for the regions with less aggressive conditions.

An alpha version of this model is provided to FDOT as a separate deliverable for evaluation and subsequent adaptation by FDOT into user-compatible platforms that may include versions for internal FDOT use and versions for incorporation in the Structures Design Manual and related documentation for a broader audience. The model receives user input on the makeup of a bridge substructure for various types of component, the structural configuration, materials of construction and service environment and develops an output consisting of the corrosion-related damage function for a period of 100 years for each Class of structural/environmental combinations and for the structure as a whole. The model version presented is intended primarily to illustrate functionality, and is subject to revision of input parameters and simplifying assumptions as appropriate before actual application.

TABLE OF CONTENTS

LIST OF FIGURES

LIST OF TABLES

LIST OF SYMBOLS

A	atmospheric zone
Ae	surface area
B	buried sub-exposure
C	chloride concentration at time t and distance x expressed as mass per unit volume of concrete
CE	counter electrode
CF	cement Factor
C_{CR}	nominal PDT-PIT crossover damage percent
C_{LTR}	nominal long-term correction ratio
Cl^-	chloride ion concentration
C_{Sli}	lowest value of chloride surface concentration
C_{Shi}	highest value of chloride surface concentration
C_0	initial chloride concentration of the bulk
C_R	chloride concentration at rebar trace at time t
C_{TA}	chloride concentration at rebar trace at time t_A
C_{TR}	chloride concentration at rebar trace at time t_R
C_S	chloride surface concentration
C_{Savg}	chloride surface concentration – average
C_{SHT}	chloride surface concentration – high tide
C_{ST}	chloride surface concentration – top
C_{Sstd}	chloride surface concentration – standard deviation
C_{SS}	chloride surface concentration – submerged
C_{SO}	oxygen surface concentration or oxygen concentration in the pore water at the external concrete surface
C_T	critical chloride threshold
C_{T0}	baseline chloride threshold value at E_{T0}
c/s	cement-sand ratio
D	apparent diffusion coefficient (cm^2/s)
D_{AVG1}	average diffusion coefficient (cm^2/s) of First Stage specimens 1-3 and 7-8
D_{AVG2}	estimated average chloride diffusion coefficient (cm^2/s) of Second Stage specimens 1-6

D_{AVGS1}	estimated chloride diffusion coefficient (cm^2/s) of secondary specimens in First Stage experiment
D_{li}	lowest value of chloride diffusion coefficient
D_{hi}	highest value of chloride diffusion coefficient
DF	damage function (%)
D_{O2}	oxygen diffusion coefficient
D_{O2T}	oxygen diffusion coefficient – top
D_{O2S}	oxygen diffusion coefficient – submerged (cm^2/s)
D_{RCM}	rapid chloride ion migration coefficient (cm^2/s)
E	steel electric potential (mV vs. SCE)
E_0	nominal equilibrium potential (mV vs. SCE)
E_{0a}	nominal equilibrium potential for the anodic reaction (mV vs. SCE)
E_{0c}	nominal equilibrium potential for the cathodic reaction (mV vs. SCE)
E_{T0}	baseline steel potential value at C_{T0}
E_{SCE}	steel electric potential vs. SCE
EIS	electrochemical impedance spectroscopy
erf	error function
F	Faraday constant
GS	galvanized steel
i_0	nominal exchange current density ($\mu A/cm^2$)
i_{0a}	nominal exchange current density for the anodic reaction ($\mu A/cm^2$)
i_{0c}	nominal exchange current density for the cathodic reaction ($\mu A/cm^2$)
i_a	anodic current density ($\mu A/cm^2$)
i_{aa}	active dissolution at a potential-dependent current density ($\mu A/cm^2$)
i_c	cathodic current density ($\mu A/cm^2$)
i_{cd}	current density under diffusional control ($\mu A/cm^2$)
i_p	steel passive current density ($\mu A/cm^2$)
i_s	net current density on the steel surface at elevation x ($\mu A/cm^2$)
IS	structural components in soil
IW:	structural components in water
L	column length

M	molar concentration (mol/L)
Nd(t)	number of elements in the entire bridge reaching damage declaration at age t
N	total number of elements in the bridge
Ni	number of elements in Class j
Nj	number of elements within each region j
OCP	OCP
P	dimensionless expression equal to Dt/a^2
P_{cum}	cumulative probability for variable n
P_{CRIT}	critical local corrosion penetration for each steel element
PDF	provisional damage function
PDT	potential-dependent threshold or chloride threshold dependent on steel potential
PIT	potential-independent threshold or chloride threshold independent on steel potential
P_{ki}	probability distribution function for variable V_k
PS	plain steel bar
r	radial direction
RE	reference electrode
R_p	linear polarization resistance
S	submerged zone
S(t)	damaged surface area at age t
SCE	saturated calomel electrode
SDG:	Structure Design Guidelines
SE:	splash evaporation zone
SF	steel factor
SS	stainless steel
T	tidal zone
t	time
t_A	time of activation
T*f*	correction factor for rebar obstruction effect
t_i	time of initiation
t_p	time of propagation

t_R:	time of removal
t_S:	time to spall
V_1	variable 1
V_2	variable 2
V_3	variable 3
V_4	variable 4
V_s	variable 5
V_k	variable k
V_n	variable n
w/c	water-to-cement ratio
x	distance along the column axis
X_C	concrete cover
X_{Cavg}	concrete cover – average
X_{Cstd}	concrete cover – standard deviation
Y	side dimension of square piles
α	radius of First Stage specimens
β_a	anodic Tafel slope
β_c	cathodic Tafel slope
β_{CT}	slope of the straight line corresponding to Eq.(1) when plotted in an E-logC_T representation. Also called the cathodic prevention slope
γ	PDT partial factor
Φ	column diameter
Φ_r	steel bar or rebar diameter
ρ	concrete resistivity
ρ_T	concrete resistivity – top of the column
ρ_S	concrete resistivity – submerged portion of the column
ρ_{High}	concrete resistivity – highest value
ρ_{Low}	concrete resistivity – lowest

1 INTRODUCTION AND OBJECTIVES

1.1 Background

Corrosion of steel in concrete is a major limitation of the durability of The Florida Department of Transportation (FDOT) bridges, especially for those in marine service. The corrosion is principally the result of chloride ion penetration through the concrete cover. The chloride ions build up at the surface of the embedded steel until reaching a critical threshold level (designated C_T) which causes breakdown of the protective passive state previously present at the steel surface. Passivity breakdown results in the onset of rapid steel corrosion with accumulation of expansive corrosion products. That accumulation creates tensile stresses in the concrete surrounding the rebar and consequent cracking and spalling of the concrete. Expensive maintenance repair and subsequent corrosion control is then needed to restore the design service life.

The FDOT has instituted corrosion prevention practices that include the use of very low permeability concrete and increased concrete cover thickness over the steel to delay chloride penetration. Those practices represent increased initial cost. Thus, accurate projection of the durability gains that may be obtained for a given initial investment is important to tailor design for the environmental conditions present at the site of a bridge, and to determine the requirements to meet the specified service life for that bridge. It is also often necessary to obtain a quantitative projection of the remaining corrosion-related service life of a structure for decision making on whether to build a new structure or continue using the existing one. The projections should be sophisticated enough to estimate not only the structure age when substantial damage will appear but also the rate at which subsequent corrosion damage would develop.

Prior research effort sponsored by FDOT under several projects (e.g., B-9119, BB-259, BA502, BC353-10, BD544-23, BC544-31) has produced corrosion damage projection models that are now routinely applied to decision making and evaluation of future performance. Briefly, the models calculate the time for initiation of corrosion based on how rapidly the transport of chloride ions (measured by the diffusion coefficient D) takes place through the concrete cover, thus establishing the amount of time needed to reach the value of C_T at the steel position. A separate estimate is made of how long after the corrosion initiation the expansive product accumulation will be enough to induce a crack or spall in the concrete. The sum of both periods yields the time to appearance of corrosion damage.[1] Since the concrete cover thickness, diffusion coefficient, surface chloride content, and even the threshold C_T vary from point to point in a bridge, damage appears earlier at some places than at others. Therefore damage develops gradually, and a statistical treatment based on the variability of the data can be used to predict the cumulative progression of that damage (the "damage function" of the structure). Predictive models based on similar principles have been produced elsewhere, for example the LIFE 365 [2] series created under sponsorship by concrete admixture manufacturers. Reflecting the need for projections tailored to the specific FDOT requirements and for a user-oriented perspective, the FDOT usually employs modeling approaches developed under its own efforts.

The presently available damage projection models used by FDOT represent a major improvement over the more qualitative approaches used in the past. However, most of those advanced models have been prepared for and used by specialists only, and have tended to address only selected combinations of critical factors without an integrated approach. A modeling approach combining an adequate blend of improvements and

reasonable simplification needed to be prepared so that FDOT can convert it into software matching that used in similar protocols at the State Materials Office.

1.2 Project Objectives and Approach

Based on the above considerations, the main objective of this project is to develop a next-generation modeling approach for projecting the extent of reinforced concrete corrosion-related damage, customized for FDOT bridges and suitable for adapting to broader use within the FDOT.

The approach used to achieve that objective consisted of:

- Identification of critical features needed for an efficient modeling approach
- Expansion of information for feature implementation in the model.
- Implementation of critical features and integration of model improvements as a practical set of instructions or working model prototype, suitable for development into software used by the FDOT in durability projections.

The following sections detail the execution of each of the approach items and the corresponding project outcomes.

2 IDENTIFICATION OF CRITICAL FEATURES AND RESEARCH NEEDS

2.1 Need for incorporating effect of prior corrosion in subsequent damage development.

2.1.1 Technical issues

Examination of the progress in prior FDOT modeling projects and of the technical literature indicated that a critical feature currently not available in practical predictive models concerns the mutual corrosion aggravation and corrosion protection effects due to existing macrocell coupling between active and passive steel assembly components. Recent work has shown that those effects can greatly affect the projected damage function for a reinforced concrete bridge. [3, 4] However, the issue was until recently largely ignored because a sufficiently simplified approach, but accurate enough for use in practical models, needed yet to be developed. Moreover, there has been a shortage of data on the corrosion threshold variation with potential. Characterization of the Potential-Dependent Threshold (PDT) is a key item in resolving this missing feature. Consequently, an experimental and modeling thrust in this project was directed to provide the necessary data, which was then incorporated into the predictive model prototype produced in the subsequent approach item.

An updated version by Sánchez et al. of a literature review by Presuel et al. on the relationship between C_T and steel potential (E) is shown in Figure 1.[5-9] Despite the scatter, Presuel-Moreno et al. noted that the general trends from a broad set of data from multiple studies followed an envelope approaching the pattern recognized in the initial investigations by Alonso et al. (blue-dashed line in Figure 1) whereby C_T increases when potentials were more cathodic than the typical open circuit potential of passive steel versus Saturated Calomel Electrode (SCE), and is relatively independent of the potential when it is more anodic than that value. [5, 10] The increase with cathodic polarization followed an exponential dependence that may be described in general terms by:[5]

$$log_{10}\left(\frac{C_T}{C_{To}}\right) \sim \frac{E_{To}-E}{|\beta_{C_T}|} \qquad \text{Eq.(1)}$$

where C_T is the threshold expressed as percentage of cement content in the concrete, E is the potential of the steel bar, while still in the passive condition, β_{CT} (named here the cathodic prevention slope), is the slope of the straight line corresponding to Eq.(1) when plotted in an E-logC_T representation (negative of the inverse of the slope of the dashed line in Figure 1), and C_{T0} is the chloride threshold value at a baseline potential E_{T0}. The latter has been chosen here to be -100 mV in the SCE scale, which is the one to be used throughout this report. This threshold-changing effect is the basis of the cathodic prevention method, whereby reinforcing steel is cathodically polarized while still in the passive condition to delay or prevent corrosion due to the elevation of the corrosion threshold. [11, 12] The redundant 3-parameter line formulation was chosen for convenience to match the form of other ruling equations in electrochemical systems. [13]

At the beginning of this project, the investigation by Alonso et al. was the only experimental assessment that focused on determining the chloride corrosion threshold dependence on potential. [10] However, those experiments used small specimens with shallow mortar cover, potentially introducing uncertainties noted in the following. An investigation by Li et al. found that the surface area of the steel is an influential parameter on the chloride corrosion

threshold, in that the greater the surface area, the smaller the obtained value of C_T tended to be.[14] Those authors strongly suggested preparing test specimens that have the largest practical steel surface area possible. Moreover, at shallow concrete layers, chloride ion penetration tends to be governed mainly by rapid permeation rather than slower diffusion, which is the usually prevalent mode of ingress of chloride ions in the systems of interest.[15] Corrosion initiation may in that case happen very fast while the chloride content of the cover layer is still evolving, leading to uncertainty in the value of chloride content determined by autopsy tests. Moreover, leaching of the thin mortar cover into the surrounding medium could introduce significant alterations in the region near the steel, possibly rendering the outcome different from that which would have been obtained with a thicker cover more representatives of field conditions. In view of those possible uncertainties and on the scarcity of data in general, a more systematic and sophisticated experimental assessment was deemed to be needed to better quantify the chloride corrosion threshold dependence on steel potential.

In addition to the experimental shortages note above, implementation of PDT in predictive models had been the subject of preliminary work but some key issues needed further attention. A previous investigation incorporated PDT in a one-dimensional finite difference deterministic model of a partially submerged reinforced concrete column by introducing Eq.(1) with the following parameter values: C_{T0}: 0.2% Cl^- by weight of cement, E_{T0}: 100 mV (SCE), and $|\beta_{CT}|$: 400 mV per decade of Cl^- (roughly approaching the dependence given by the dashed line in Figure 1).[3]

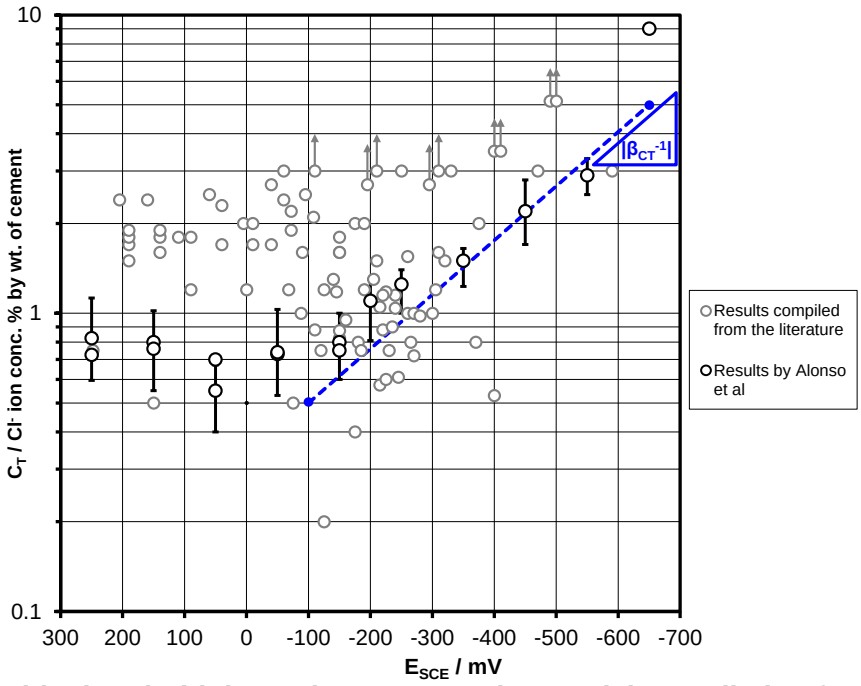

Figure 1: Chloride threshold dependence on steel potential compilation from the literature by Presuel et al. [5] and updated by Sánchez et al. [6]

As will be shown in more detail in Section 4.3, in the model to predict damage development incorporating PDT, in the preliminary work corrosion was assumed to start when C_T was reached in a steel zone (or node) of a given size. That event resulted in activation of that zone and the creation of a macrocell corrosion pattern where that zone was anodic while the rest of the steel in the column remained passive, namely a cathodic zone. The corrosion macrocell pattern for that configuration was then calculated to obtain the value of the steel potential E at every zone in the system. The still passive steel zones, near that first activated site developed a significantly more negative value of E than the one present before the first activation event. Hence, those zones were assigned per Eq.(1) a correspondingly larger value of C_T than before. Consequently, corrosion initiation in those regions was delayed. As the new C_T value was eventually reached in other zones, the macrocell pattern was affected accordingly and corrosion development was delayed in nearby regions as well. The overall result was a much slower progression of corrosion damage in the system than if the C_T would have been a constant value, potential-independent value ($|\beta_{CT}| = \infty$). The effect, illustrated in Figure 2, was found to be a dramatic decrease in the predicted amount of corrosion damage when $|\beta_{CT}|$ was a finite value compared to the case of a potential-independent threshold $|\beta_{CT}| = \infty$.

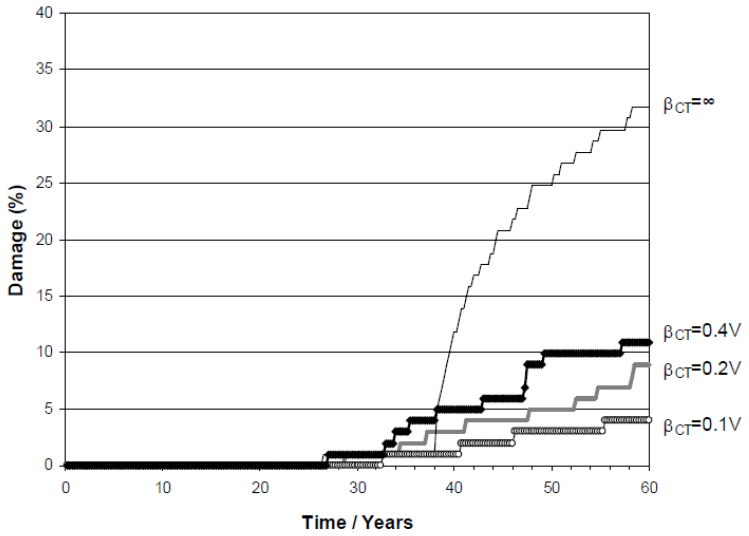

Figure 2 Damage projections in previous model calculations showing strong decrease in projected damage at age=60 years when comparing the case of a potential independent threshold ($|\beta_{CT}| = \infty$) and cases where C_T depended on potential of the passive steel.[3]

Moreover, Figure 2 shows that the amount of projected damage can be quite sensitive to the value of $|\beta_{CT}|$, where the corrosion damage was evaluated using values of $|\beta_{CT}|$ = 100, 200 and 400 mV per decade of Cl^- concentration. Thus, for engineering forecasting purposes, more accurate parameter choices (especially for $|\beta_{CT}|$) were desired for a better representation of a marine structure, further justifying the need for added experimental work indicated above.

The initial predictive model incorporating PDT served to demonstrate the feasibility of the concept; however, in addition to the dependence on $|\beta_{CT}|$ the damage prediction was found to be highly sensitive to the assumed size of the corrosion activation zone (or node). As the size of the activation zones was made smaller, the total predicted amount of damage at a

given age decreased toward a zero limit value. As explained in Ref. [3] that result was not consistent with the trends expected from basic considerations on the behavior of the system, and resolution of the issue was a major issue to be cleared before further developing the concept. Examination of the model assumptions suggested that the problem stemmed from neglecting the local resistance of the concrete around the steel bars. As a result, the macrocell coupling effect was inappropriately exaggerated as node spacing decreased leading to an erroneous limit condition. A solution was therefore needed, by implementing an improved formulation that would account for the local resistance polarization consistent with the size of activation zone.

2.1.2. Summary of needed work to improve technical issues

The above discussion identified the needs to incorporate efficiently the effect of prior corrosion in subsequent damage development by first, providing additional evidence on the extent and nature of the PDT phenomenon, using test specimens built with sizable dimensions with mortar and concrete, and obtaining a more solid indication of the value of $|\beta_{CT}|$ under experimental assessments, so as to reduce uncertainty about the extent of the effect of incorporating PDT in the model to be prepared under this project. Information to address those needs was developed in experiments in this project, with findings described in Chapter 3.

The discussion in section 2.1.1 also identified the need to solve the modeling issue concerning the uncertainty on the model sensitivity to activation zone size. This need was also addressed in this project by computations, with results provided in Chapter 4.

2.2 Need for accounting for multiple exposure zones in a structure.

2.2.1 Technical Issues and summary of needed work that was conducted in this project.

In discussions with project management, it emerged that FDOT needed also a modeling approach that accounts for the increasing emphasis on component design, in which different portions of the same bridge are designed to best adapt to the local corrosion environment. Thus, previously, an entire bridge may have been classified as being in an extremely aggressive environment with consequent cost for added corrosion protection design everywhere. With component design and a customized corrosion modeling approach, some portions of the same bridge may be found to require less costly concrete formulation and cover specifications and still perform adequately.

To avoid excessively conservative design, model improvements were needed including consideration for various exposure regimes within a given bridge as identified in the FDOT Structure Design Guidelines and related sources.

This need has been addressed through the model development detailed in Chapter 4, which includes provision for multi-elevation and multi-environment features in the prototype model further detailed in Appendix 1.

3 EXPANSION IN INFORMATION FOR FEATURE IMPLEMENTATION - EXPERIMENTAL INVESTIGATIONS.

The experiments to provide additional evidence of the extent and nature of the PDT phenomenon, using sizable test specimens built with mortar and concrete, and to obtain a more solid indication of the value of $|\beta_{CT}|$, were conducted in two stages. The First Stage consisted of preliminary tests using specimens with moderate steel surface area embedded in mortar and in a continuous immersion regime.[6] The Second Stage involved concrete specimens with large steel surface area and an alternating wet-dry exposure regime more representative of actual service conditions.[16] Both stages and their findings are described in the next sections.

3.1 First Stage - Mortar Tests with Moderate Steel Surface Area

3.1.1 Materials and Experimental Setup

Cylindrical mortar specimens with an embedded type #5 rebar were submerged in a saturated NaCl (5.33 M) solution, as shown in Figure 3.[17] Plain A-615 rebar with high temperature mill scale on the surface was used.[18] The top and bottom of the rebar was coated with an epoxy resin, to prevent corrosion initiation in these areas. Ordinary Portland Cement Type I/II was used with a water-to-cement ratio (w/c) of 0.6 and a cement-sand ratio (c/s) of 1/3. The cement factor (CF) was 488 kg/m^3. The average mortar cover thickness of the rebar was 1.6 cm and it had an exposed area of 32 cm^2. An embedded activated titanium reference electrode (RE), periodically calibrated with respect to SCE, was used for potential control in each specimen. [19] The top and the bottom of the mortar specimens were also covered with a layer of epoxy to avoid chloride ingress in those mortar regions. The specimens were cured for 7 days at high humidity before being placed in the exposure container.

One set of duplicate specimens was exposed at the open circuit potential (OCP) and three other sets were cathodically polarized at -200, -400 and -600 mV (SCE), respectively, representing potentials of passive steel in string macrocell contact with adjacent fully corroding steel. The solution had also addition of $Ca(OH)_2$ in excess of its solubility limit to maintain an average pH of ~>12 and minimize alkaline leaching from the mortar. A counter electrode (CE), mixed metal oxide (MMO) deposited in a titanium mesh, was placed under the submerged specimens. A tight lid minimized access of external air and CO_2 to the solution, but sufficient oxygen existed in the container for the solution to be considered as being naturally aerated. A multiple potentiostat was used to adjust the potential for the polarized specimens and periodically corrected with a SCE as needed to stay within ±10 mV of the target value. The experiment was conducted in a climate controlled laboratory with an average temperature of 21ºC. While developing the First Stage experiment procedure, additional supplemental tests were conducted with a limited number of specimens made with 0.5 w/c mortar and a CF=513 kg/m^3, and exposed to a solution with NaCl content changed stepwise from 0.5 M (day 0) to 1 M (day 36 on). Methodology was otherwise similar to that used for the other specimens. Four of the supplemental specimens experienced activation during the test period and the results are noted together with those of the First Stage experiments.

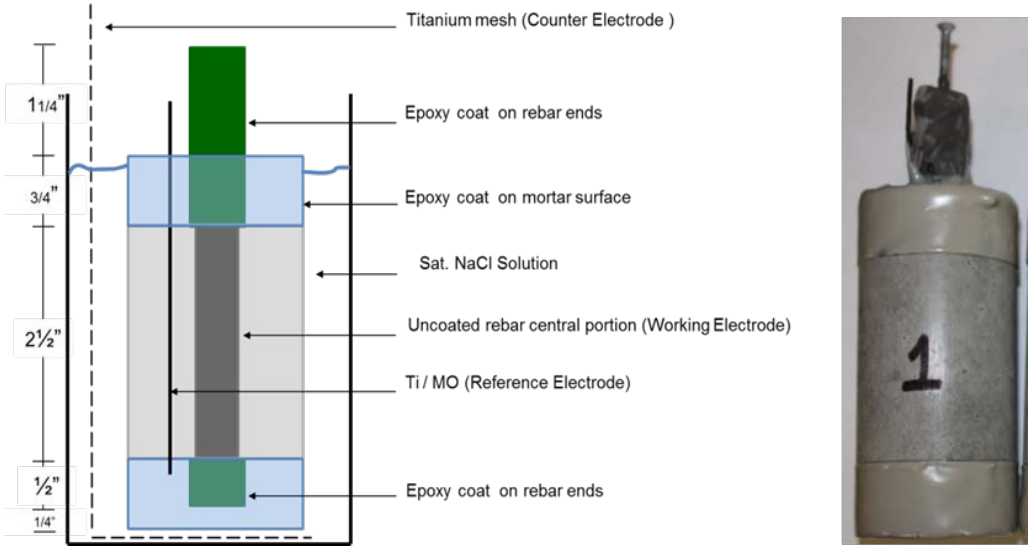

Figure 3 First Stage Experiment Specimen Layout

3.1.2 First Stage Results

3.1.2.1 Open Circuit Specimens

Time of activation t_A or time when corrosion starts was estimated by observation of the potential evolution measurements and through electrochemical impedance spectroscopy (EIS) trends. The Nyquist plots (Figures 4a and 4b) suggest that the interfacial EIS behavior approximated that a simple constant phase element (CPE) – polarization resistance (R_p) parallel combination. At short exposure times, the value of R_p was large but later on there was a sharp transition to smaller values indicative of the onset of active corrosion. The OCP downward trend was consistent with that behavior. From observation of Figure 4c, the transitions took place at around the time that the OCP reached -300 mV (SCE), so that exposure duration (13 and 24 days for specimens 7 and 8, respectively) was declared to correspond to the corrosion initiation event for the present purposes.

3.1.2.2 Cathodically Polarized Specimens

The polarized specimens initially demanded cathodic currents commensurate with the extent of cathodic polarization imposed as shown in Figure 5. As time progressed, the absolute value of the cathodic current in the -200 and -400 mV (SCE) specimens decreased appreciably, indicative of the onset of diffusion-polarized regimes for those cases. Current demand was very small for the specimens polarized to -200 mV (SCE), which are likely to have remained near activation-polarized conditions for the cathodic reaction. Activation was manifested for the polarized specimens by a shift in the polarizing current from a cathodic to an anodic regime. Reaching an anodic current greater than 0.2 $\mu A/cm^2$ was chosen as the criterion for the onset of the active regime, following the criterion used by Alonso et al. [11] The transitions for the polarized specimens that experienced activation during the exposure period are shown in Figure 5.

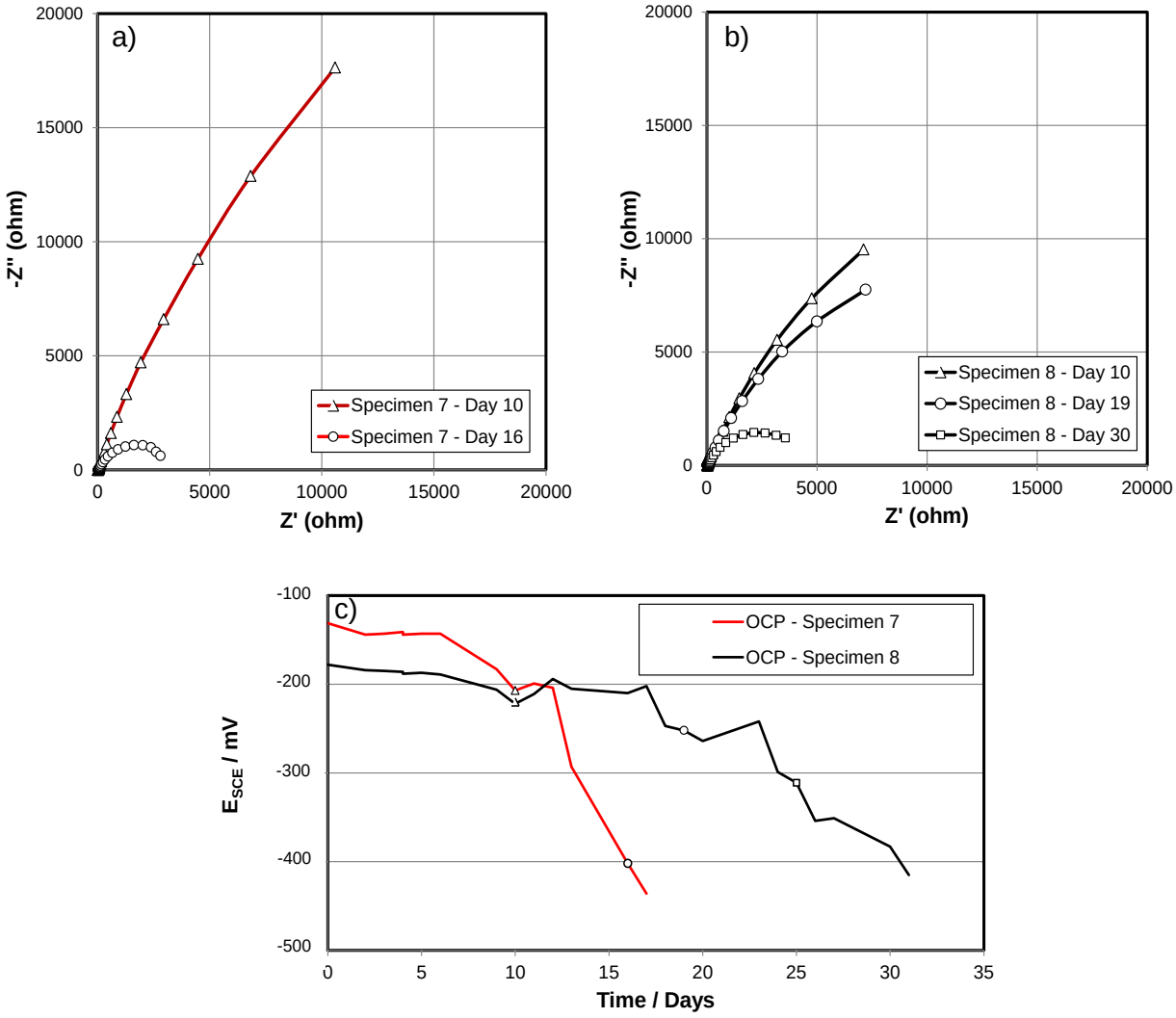

Figure 4: Time trends for OCP specimens. a),b): Nyquist diagrams (lowest frequency shown 1 mHz; 5 data points per frequency decade) keyed to symbols in OCP graphs. c): Potential evolution.

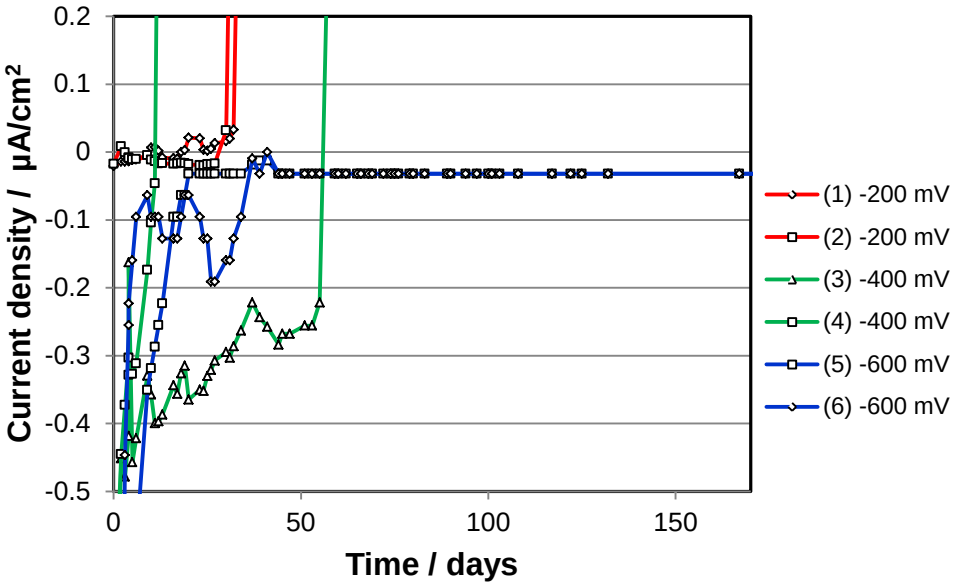

Figure 5: Applied current density (anodic is >0) vs time for each polarized specimen at the indicated potential

3.1.2.3 Estimation of chloride content at the rebar at the time of corrosion initiation

After demolition, a 1 cm masonry drill was used to obtain mortar samples with no corrosion products at the rebar trace for chloride analysis Acid-soluble chloride concentration of 1-gram mortar powder samples duplicates for each specimen was determined following the "Florida Method of Test for Determining Low-Levels of Chloride in Concrete and Raw Materials".[20] The chloride concentration values were expressed in the form of total chloride content by weight of cement.

Because of the confirmatory time lag between the time of specimen activation and that of extraction, the chloride content at the time of sampling of the rebar trace was usually greater than that upon activation. A correction procedure was developed by assuming on first approximation simple cylindrical diffusion governed by Eq.(2), an expression of simple Fickian one-dimensional diffusion in cylindrical coordinates:[21]

$$\frac{\partial C}{\partial t} = \frac{1}{r}\frac{\partial}{\partial r}\left(rD\frac{\partial C}{\partial r}\right) \qquad \text{Eq.(2)}$$

where D is the apparent chloride diffusion coefficient, which is time and space invariant, r is the radial dimension, and t is time. The boundary conditions assumed a constant surface chloride concentration (C_S) at the outer cylinder wall and a zero-flux condition at the rebar surface, thus accounting for the rebar obstruction effect for chloride accumulation at the rebar trace.[22, 23] The solution of Eq.(2) was obtained by the Finite Difference Method (FDM). The equation was formulated in terms of dimensionless expressions: $P=Dt/\alpha^2$, C_{TR}/C_S and r/α; where C_{TR} and α are chloride concentration at the rebar trace at a specific

time and radius of the specimen, respectively. The output to the problem was the numerical functional relationship between C_{TR}/C_S and P.

A representative value of C_S was obtained following a similar procedure as for the rebar trace, but instead sampling the outer cylinder surface. The chloride content measured by chemical analysis at the rebar trace (C_{TR}) at the time of removal (t_R) was then divided by C_S to obtain $C_{TR}/C_{S,}$ which in turn yielded $P(t_R)$ (P at the t_R) per the functional relationship determined above. With the values of t_R, $P(t_R)$, and a, an estimate of D was obtained, which was then used to obtain $P(t_A)$ and from similarly obtain an estimate of C_T, the concentration at time of activation, which is the reported threshold value.

Samples of the outer surface of specimens 5 and 6 (see Table 1 for specimen condition) that were analyzed to determine C_S yielding values respectively of 41 kg/m^3 and 40 kg/m^3, respectively, with an average of 40.5 kg/m^3. This value is generally consistent with the expected high porosity of the mortar, given its high w/c ratio and an assumption of pores near the surface filled with the saturated NaCl solution plus some extent of chloride binding by the surrounding matrix.[24, 25] For specimens 5 and 6, as of day >170 no activation events were observed. A lower bound for rebar trace chloride concentration was estimated by assuming that the value of D was the same as the average D_{AVG1}, 2.43 $\times 10^{-7}$ cm^2/s, of the rest of the specimens and using the C_{TR}/C_S – P relationship to estimate C_T at the latest exposure time. For that long exposure, the resulting C_T value was nearly equal to the C_S value.

For the specimens from the supplemental tests (S2, S4, S7, S8), only activation time data were available. A rough estimate of C_T was made nevertheless in those cases by a similar procedure as used for specimens 5 and 6. Nominal values of C_S and D were assigned as follows. The surface concentration was assumed for simplicity (neglecting adjustments for porosity and chloride binding differences) as being directly proportional to the solution chloride content, prorating directly from the C_S value used for the First Stage tests, and further using a constant nominal weighted value based on the fraction of t_A spent in the 0.5 M and 1 M regimes. Since in the supplemental tests a 0.5 w/c mixture had been used, the corresponding value of D was estimated from the average value from the main test sequence, and multiplying it by the average ratio of D (0.5 w/c) to D (0.6 w/c) obtained from work by previous authors resulting in D_{AVGS1}.[26-28]

3.1.2.4 First Stage Potential-Dependent Threshold findings

Table 1 summarizes the results and calculations of each test condition. The values for D estimated from the First Stage test sequence were generally high, consistent with those expected for high w/c mortar in a wet environment.[26-28] It is noted that the estimated value of D for specimen 4 was significantly higher than for the others, reflecting the high chloride content measured at the rebar trace of that specimen after a relatively short exposure period and the consequent early activation as well. It is speculated that mortar consolidation may have been poorer in that sample, although there was no readily visible sign of deficiency. Regardless of the early chloride buildup, the results for this specimen nevertheless followed the same overall trends discussed next. It is recognized that the results from the supplemental tests represent only rough estimates, provided here primarily for completeness.

Table 1 Calculations and results for each First Stage test condition.

Specimen	Potential (mV)	t_A (day)	t_R (day)	C_{TR} (kg m^{-3})	D (cm^2 s^{-1})	C_T (kg m^{-3})	C_T (% by wt. of cement)
1	-200	34	45	9.47	1.37×10^{-7}	5.4*	1.10*
2	-200	31	31	4.00	1.35×10^{-7}	4.0*	0.83*
3	-400	59	60	15.31	1.40×10^{-7}	15*	3.06*
4	-400	12	13	14.03	6.09×10^{-7}	13*	2.62*
5	-600	>170	>170	-	D_{AVG1}	>40**	>8.1**
6	-600	>170	>170	-	D_{AVG1}	>40**	>8.1**
7	-150	13	17	5.34	2.75×10^{-7}	2.5*	0.52*
8	-190	24	31	6.68	1.66×10^{-7}	3.4*	0.69*
S2	-200	117	-	-	D_{AVGS1}	5**	1**
S4	-400	152	-	-	D_{AVGS1}	6**	1.1**
S7	-120	51	-	-	D_{AVGS1}	1.7**	0.3**
S8	-90	63	-	-	D_{AVGS1}	2.5**	0.5**

Notes:
D_{AVG1}: Estimated diffusion coefficient 2.43×10^{-7} cm^2/s = average of values from specimens 1-3 and 7-8.
D_{AVGS1}: Estimated diffusion coefficient 1.56×10^{-7} cm^2/s = value obtained from the conversion of D at w/c 0.6 to D w/c 0.5, as described in text.
* Corrected from direct measurement to account for time lag between activation and extraction.
** Lower bound values of C_T estimated for non-activated specimens
Roundoff applied to finished values; internal table computations conducted with additional digits.

3.2 Second Stage - Concrete Tests with Large Steel Surface Area

3.2.1 Materials and Experimental Setup

A modified version of the ASTM G109 “Standard Test Method for Determining Effects of Chemical Admixtures on Corrosion of Embedded Steel Reinforcement in Concrete Exposed to Chloride Environments” was used as a basis to prepare a set of twelve reinforced concrete slabs 66 cm long, 10.16 cm wide and 6.35 cm high, exposed to a ponding regime while under potentiostatic control.[29] Layout of the side and top view of the modified standard version is shown in Figure 6

The concrete cover thickness X_C of the embedded steel rebar was 2 cm. A single rebar was used, size #5 plain steel ASTM A-615-09B Grade 60 with an undisturbed gray mill scale. A stainless steel bolt screw, with two washers and a nut were tapped to one end of the steel bars to later connect the steel to the potentiostat after casting and curing. Next, the steel bar ends (5 cm) were also coated with epoxy, similar to the First Stage tests, to prevent corrosion in these regions. The uncoated steel area was ~300 cm^2, approximately an order of magnitude greater than in the First Stage.

Unlike the specimen configuration in ASTM G-109, the steel bar embedded in each specimen was intended to be cathodically polarized (except those at the OCP condition) with a potentiostat, as mentioned above. For that reason, a 5 cm embedded activated titanium RE, frequently calibrated with respect to an external SCE, was placed parallel to the steel bar. The CE, same material used as in the First Stage as well, was placed on either

side parallel to the length of the steel bar. The CE was held to Plexiglass rods to prevent any contact with the working electrode.

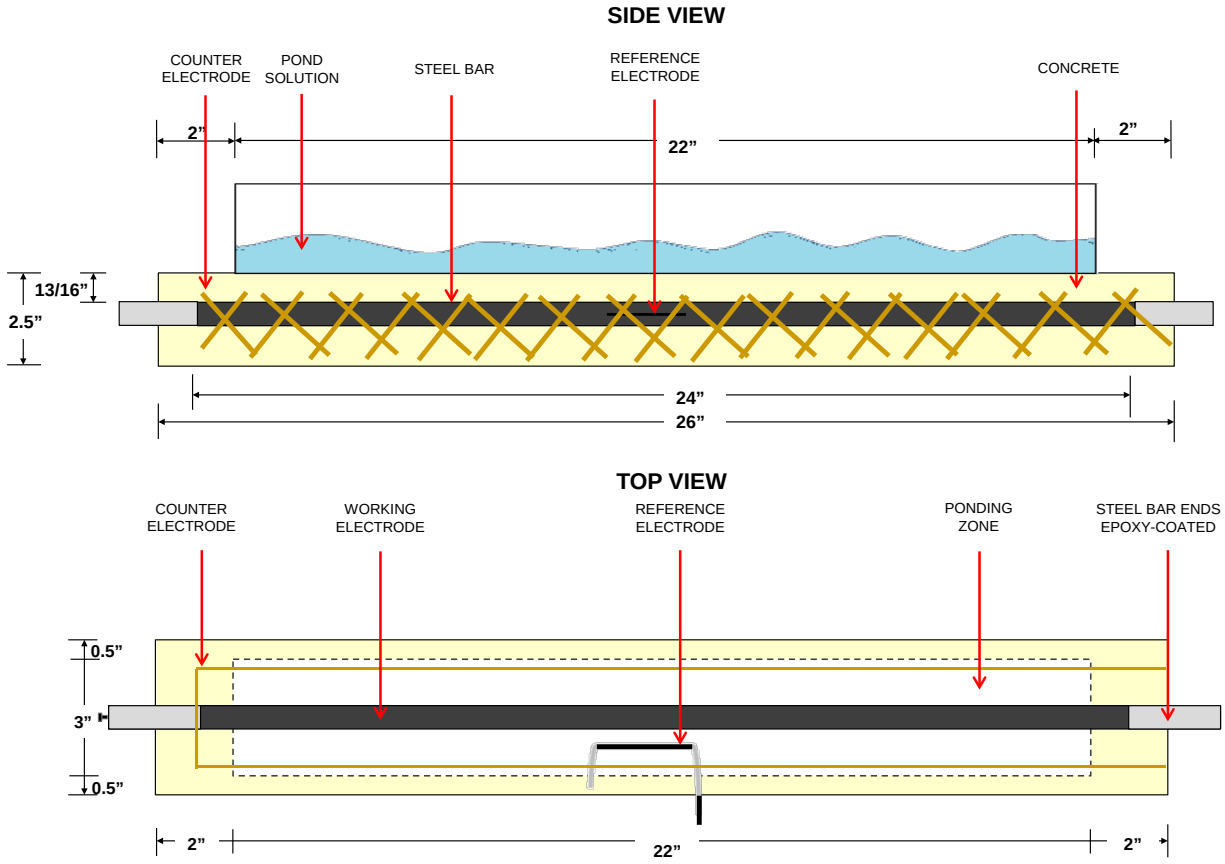

Figure 6: Side and top view of the reinforced concrete specimens

A 2D model was developed using Comsol Multiphysics to find optimal position for the CE placement by minimizing the variability of the potential at the steel surface between the upper and lower arrowed points as illustrated in Figure 7. The modeling results showed that the configuration on the left-hand side of the figure, CE placed under the steel bar, resulted in a larger electric potential (red font numbers) difference between the arrowed points, compared to the CE configuration on the right hand side. In the latter, the CE placed in a position parallel to the embedded steel bar yielded an electric potential difference as little as ~0.003 V, indicating a uniform current flow along the steel bar. Hence, the right hand side configuration in Figure 7 was used to build the specimens.

Casting molds were built out of wood as shown in Figure 8. Prior to casting, the electrodes were placed in the molds and the interior wood was covered with mineral oil, assuring no contact with the soon-to-be embedded electrodes. Ordinary Portland Cement Type I/II was used with a water-to-cement ratio (w/c) of 0.6 and a cement-to-sand ratio (c/s) of 2.2. The coarse aggregate used was #89 limestone. The cement factor (CF) was 455 kg/m^3.

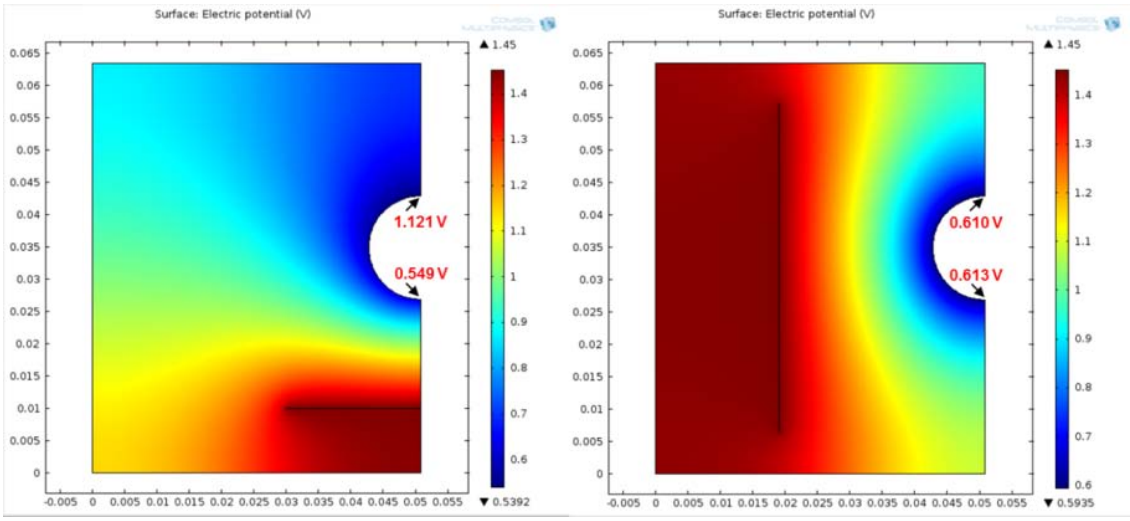

Figure 7 Modeling results to find optimal position for counter electrode placement

The reinforced concrete specimens were cured for 32 days at high humidity. After curing, a pond built with Plexiglass and sealed with marine adhesive was placed on top of each slab (similarly as in Ref.[6] to recreate wet and dry regimes. Fresh water was ponded continuously during the first 17 days for leak proofing and stabilization. During this period, the exterior faces of the specimens were coated with epoxy as shown in Figure 9, leaving the bottom region uncovered. Stainless steel bolt screws were attached to the two outer ends of the CE to subsequently connect the two embedded meshes with a wire. Afterwards, regular wet-dry ponding took place; during the wet cycle (3.5-day period) a solution of 4 M NaCl was placed in the pond, a lid was placed on top of the pond to prevent evaporation. The solution was removed for the dry cycle (3.5-days too).

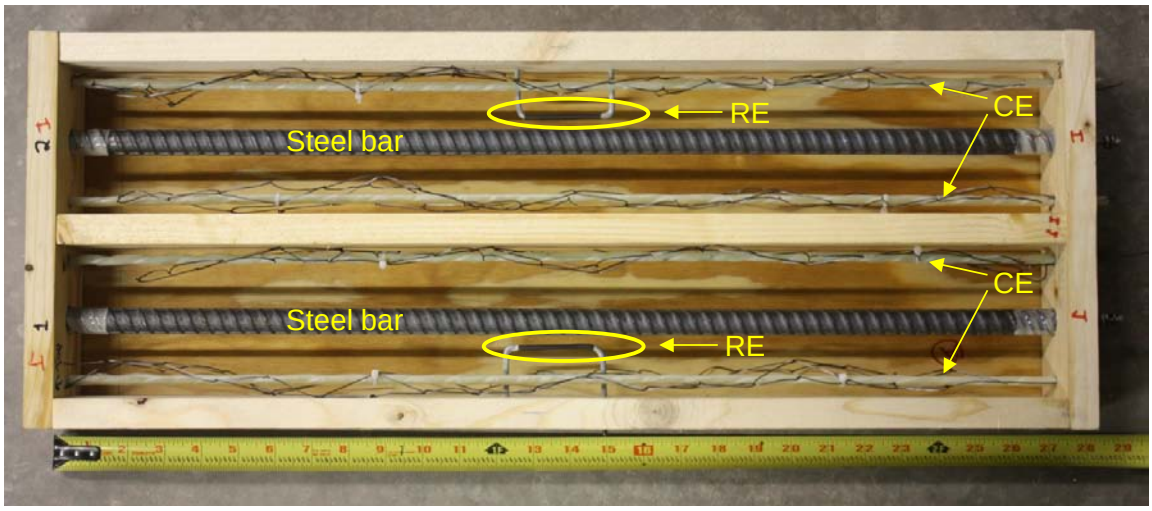

Figure 8: Second Stage Specimens prior to concrete casting. RE: reference electrode. CE: Counter Electrode

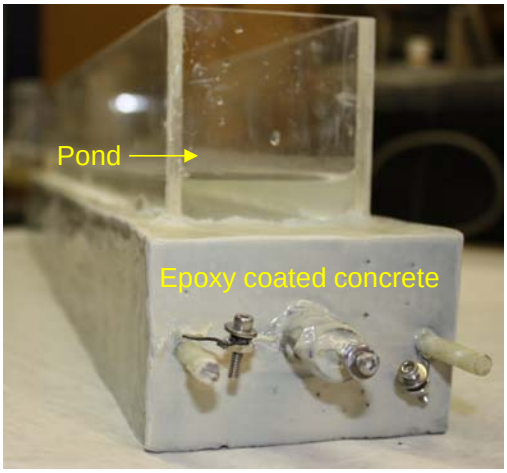

Figure 9: Specimen after placing the pond and applying epoxy

A set of triplicate specimens were tested at the open circuit potential (OCP) and three additional triplicate sets were cathodically polarized at -200, -400 and -600 mV (SCE), respectively, as shown in Figure 10. The evolution of the steel potential was measured periodically for all the specimens using the embedded RE and a SCE. EIS tests were performed periodically as well, for the OCP specimens only. A frequency range of 1 mHz to 1 MHz with an amplitude of 0.010 V rms was used. The Echem Analyst software by Gamry Instruments was used to model and estimate the Polarization Resistance (R_p) value of the embedded steel bar. The R_p value was calculated assuming a circuit that has a solution resistance, a non-ideal interfacial capacitance and polarization resistance parallel combination.

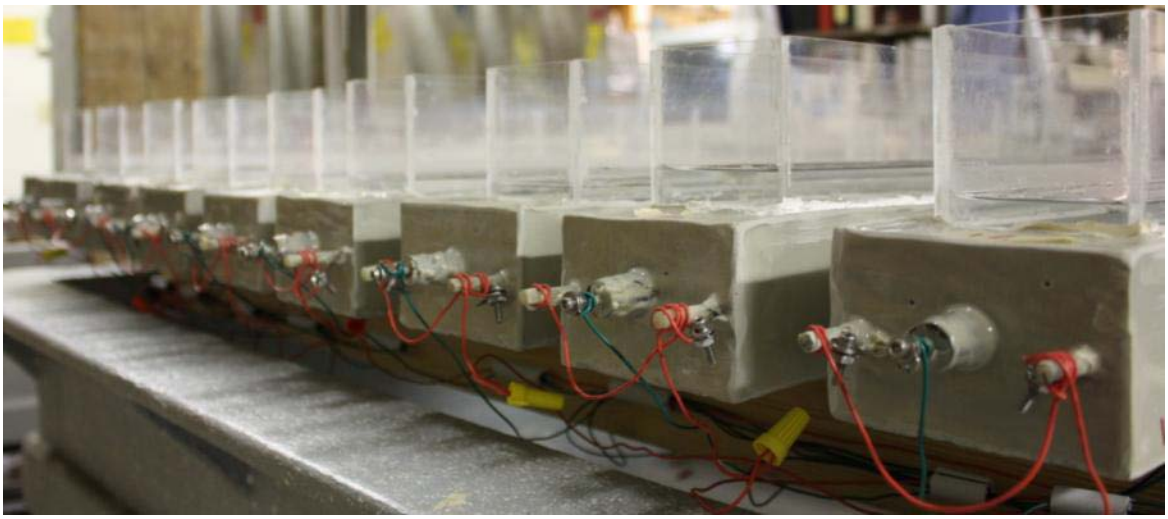

Figure 10: Cathodically Polarized Specimens

3.2.2 Second Stage Results

3.2.2.1 Open Circuit Specimens

When the salt water ponding regime exposure was initiated (day zero) the steel potential readings were around -80 mV (SCE) and remained so for about 150 days as it is shown in Figure 11. Approximating the usage for the First Stage experiments, the time of corrosion initiation (or activation) t_A for the Second Stage experiments was deemed to be confirmed when a steel potential < -200 mV (SCE) was reached. As a secondary confirmation of steel activation, the value of R_p was observed to have exhibited about one order of magnitude decrease compared to the value when the embedded steel was in the passive condition.

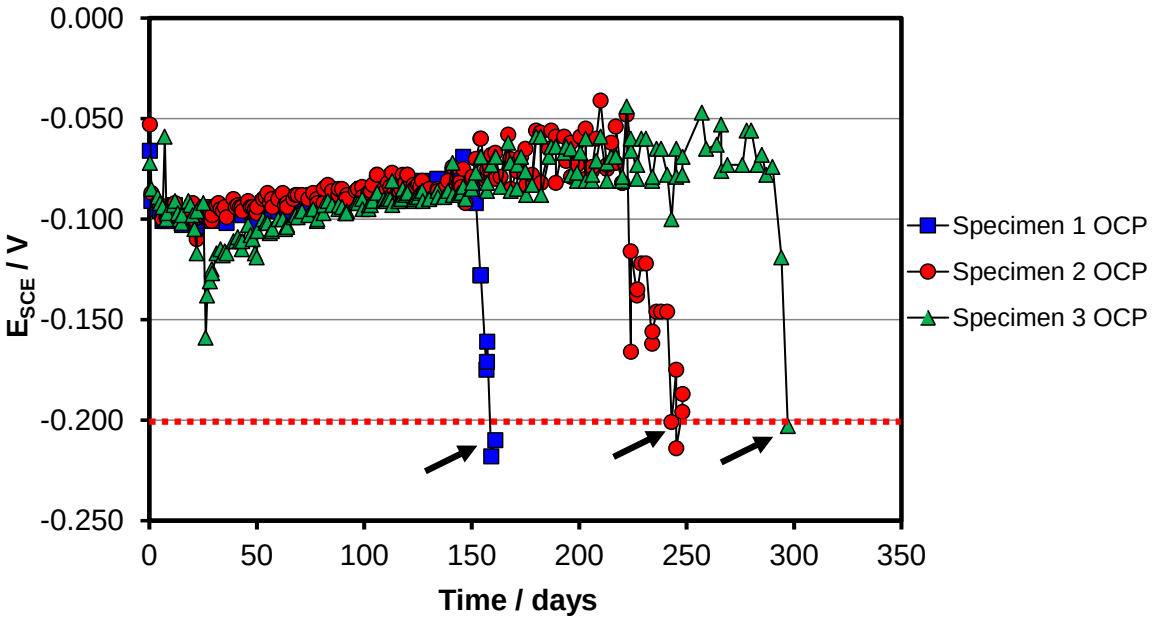

Figure 11: Evolution of the steel potential for the Second Stage OCP specimens. Arrows indicate activation event declaration.

The activation events for the OCP specimens are indicated by the arrows in Figure 11. The average activation time for the triplicate set was 235 days. The specimens were retained sometime after the activation events occurred to validate corrosion initiation through EIS tests. An example of Nyquist plot results is shown for specimen 1 in Figure 12. During the first 150 days the embedded steel bar maintained an R_p value of ~20,000 ohms. Twenty days later, a potential drop to -0.170 V vs SCE was measured and a pronounced reduction of the semi-circle diameter on the Nyquist plot was observed with an R_p value of ~4000 ohms. The activation time was declared on day 161, when the steel potential passed the -200 mV mark with a reading of -220 mV (SCE). EIS test resulted in an R_p of ~2,000 ohms, validating the time of activation estimated from OCP measurements.

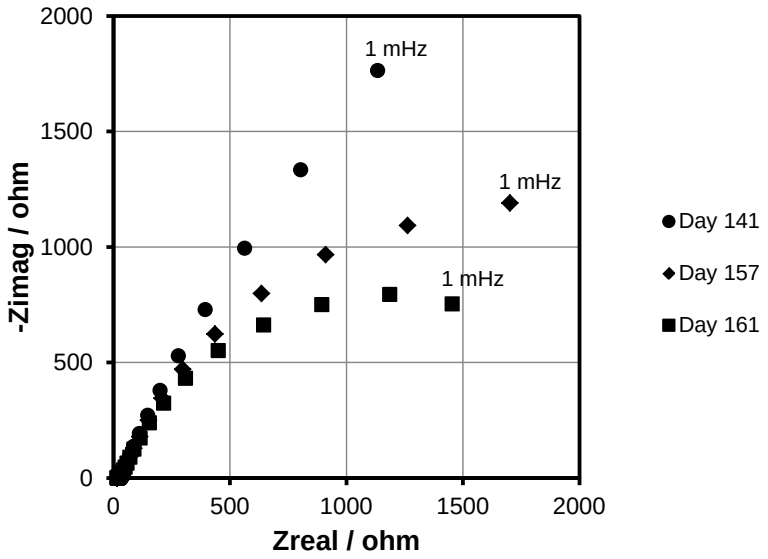

Figure 12: Time progression of EIS for specimen 1 at OCP condition, indicating marked reduction in R_P on activation at day 161. Nyquist representation; 5 data points per frequency decade.

3.2.2.2 Cathodically Polarized Specimens

The current demanded by the polarized specimens was initially negative (cathodic) when the embedded steel bar potential was set towards negative values (-200, -.400 and -600 mV (SCE)). Following the methodology of the First Stage, the moment of activation was declared when the demanding current density reached a value greater than +0.2 μA/cm^2. An example of this procedure for specimen 6, polarized at -200 mV (SCE) is shown in Figure 13. The red dashed line and the black arrow corresponds to the activation criterion and event, respectively. Fluctuations were observed during the cathodic-anodic current transition as shown in Figure 13, thus specimens were kept polarized for a period afterwards to confirm activation.

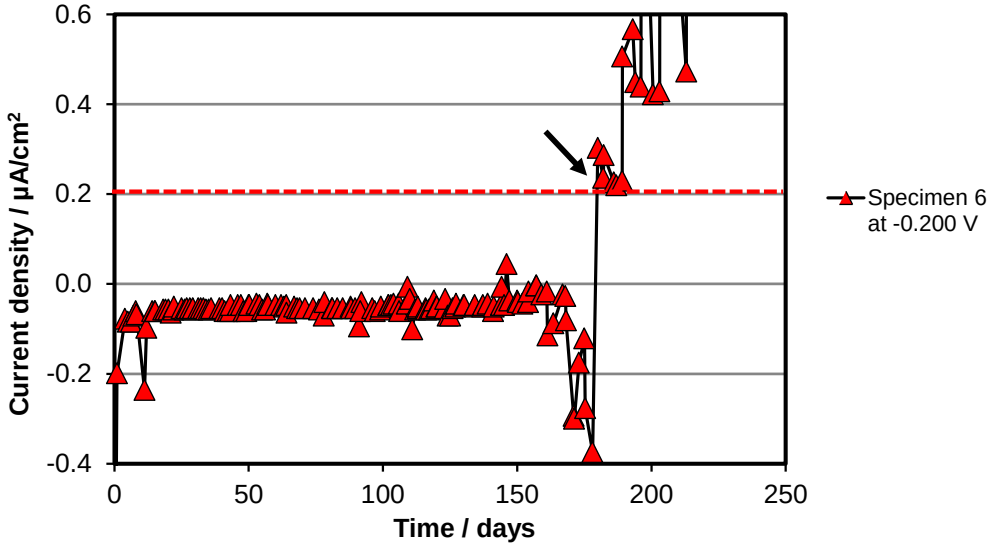

Figure 13: Current density with respect to time for a specimen cathodically polarized at -200 mV

3.2.2.3 Estimation of chloride content at the rebar at the time of corrosion

Once activation was confirmed, the specimen was removed from the experimental setup and sliced with a masonry saw on the sides until reaching approximately ~3 mm away from the rebar. A chisel and hammer were then used to break the specimen into two halves. The top part of the specimen was then wedged away from the rebar exposing the rebar trace for the concrete-rebar interface closest to the pond (see Figure 14). The rebar trace was milled using a masonry drill 1 cm diameter similar to the procedure described in the First Stage specimens. The milling depth was ≤ 2 mm, and normally 9 grams of concrete powder were collected avoiding regions where corrosion products were observed. Triplicates of 3-gram concrete powder sample were analyzed for chloride ion concentration following the same procedure as mentioned in the First Stage methodology, the results averaged for a reported result (Table 2).[20]

When specimen 7 was processed, large amounts of corrosion products were observed along the concrete rebar trace; and as a result, an insufficient amount of concrete powder (only about 1/3) was collected to meet the recommendation given in the FDOT FM5-516.[20]. Consequently, the reported result for that specimen was for a single (not average of triplicate tests) value and subject to corresponding uncertainty. That value was unusually large and suggestive of an artifact.

The chloride content at the concrete ponding surface C_S was determined for selected specimens following a similar procedure as that indicated above for the trace. The results were 20.2 kg/m^3 and 22.4 kg/m^3 for specimens 2 and 3, respectively. The average value, 20.2 kg/m^3, was used as the fixed C_S value for all specimens in the calculations explained in the next section.

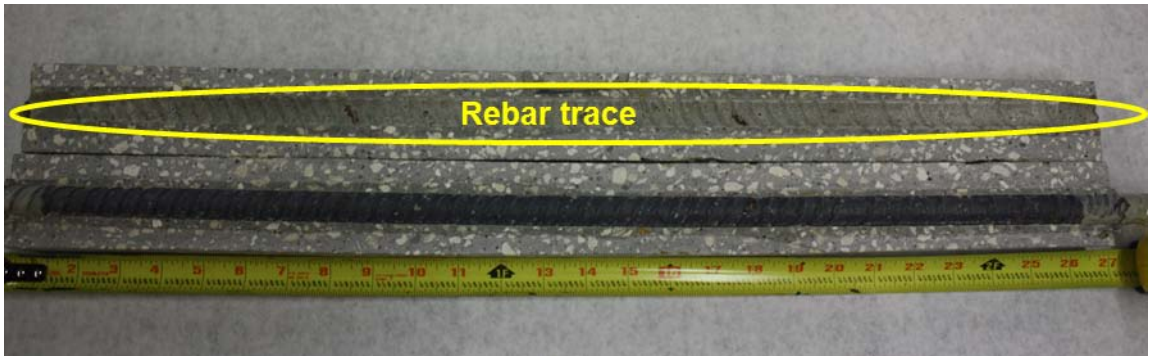

Figure 14: Reinforced concrete specimen after autopsy.

The procedure yielded the chloride ion concentration C_{TR} at the time of specimen removal t_R. An adjustment for time delay was conducted to estimate the concentration C_T at the declared time of activation (t_A). The adjustment was calculated assuming simple diffusion in a semi-infinite[(1)] plane sheet with invariant C_S, C_0 and D (Eq.(3), but correcting for the presence of the steel bar (diameter Φ_r) with clear cover X_C as described in a computational investigation by Kranc et al.[22, 23] That work shows that for the above conditions the concentration C after a time of exposure t at the point of the rebar surface, closest to the external surface is given by

[(1)] The domain is actually of finite thickness, but since it is about 3 times greater than X_C, the behavior at the relatively early stages considered here approximates conditions in a semi-infinite domain.

$$C = C_S\left(1 - erf\frac{X_C}{2\sqrt{Dt/Tf}}\right) \quad \text{Eq.(3)}$$

where T*f* is a derating factor that is a function of the ratios Φ_r / X_C and C/C_S (note the formulation as expressed in Equation 2 is implicit on C). For the present case $\Phi_r/ X_C = 0.77$, a fixed value. Processing accordingly the graphic solutions to Eq.(4) given by Kranc for that ratio value shows that T*f* can be approximated by: [22]

$$Tf = -0.65\frac{C}{C_S} + 0.792 \quad \text{Eq.(4)}$$

Using the global values of C_S and X_C and taking for each specimen $C=C_{TR}$ and $t=t_R$, the corresponding value of D was calculated by clearing it from Eq.(4), with results shown in Table 2.

3.2.2.4 Second Stage Potential-Dependent Threshold findings

Table 2 shows the results of the Second Stage experiments. Results for specimens 1-6 were quite consistent with each other (average 5.14×10^{-8} cm^2/s, standard deviation 1×10^{-8} cm^2/s) and in the expected range for a highly permeable concrete as used here. Due to the uncertainty associated with the chloride content of specimen 7 as mentioned earlier, two alternative values of C_T were presented as a range in Table 2. The first value was calculated using and average value of D (D_{AVG2}) obtained for specimens 1-6 together with Eq.(3) and Eq.(4) to obtain a numerical estimate of C_T. The second value involves no adjustment procedure, so C_T was taken to be nominally equal to C_{TR}. Five of the cathodically polarized specimens did not experience corrosion activation up to day 600, as mentioned earlier. Exposure continues, but a nominal bounding lower value of C_T was obtained following the same method as that used to obtain the second alternative for specimen 7.

Table 2 Calculations and results for each Second Stage test condition.

Specimen	Potential (mV)	t_A (day)	t_R (day)	C_{TR} (kg m^{-3})	D (cm^2 s^{-1})	C_T (kg m^{-3})	C_T (% by wt. of cement)
1	-100	161	180	4.10	5.38×10^{-8}	3.45	0.76
2	-100	243	250	6.20	5.34×10^{-8}	6.01	1.32
3	-100	297	327	6.02	3.98×10^{-8}	5.37	1.18
4	-200	335	347	6.06	3.77×10^{-8}	5.82	1.28
5	-200	213	222	6.64	6.40×10^{-8}	6.35	1.39
6	-200	189	222	6.18	5.99×10^{-8}	5.09	1.12
7	-400	320	347	20.6	-	7.7*-20.6	1.7*-4.5
8	-400	900	-	-	D_{AVG2}	14.1**	3.09**
9	-400	900	-	-	D_{AVG2}	14.1**	3.09**
10	-600	900	-	-	D_{AVG2}	14.1**	3.09**
11	-600	900	-	-	D_{AVG2}	14.1**	3.09**
12	-600	900	-	-	D_{AVG2}	14.1**	3.09**

Notes:
D_{AVG2}: estimated average chloride diffusion coefficient obtained from specimens 1-6
*Value of C_T estimated using average value of D from specimens 1 to 6 ($D_{AVG2}=5.14 \times 10^{-8}$ cm^2/s)
**Lower bound values of C_T estimated with D_{AVG} for specimens non-activated specimens
Roundoff applied to finished values; internal table computations conducted with additional digits.

3.3 Discussion of First and Second Stage experimental findings

The experimental results from the First and Second Stage are represented by the red symbols in Figure 15. The C_T values are expressed in total chloride content by weight of cement in the y-axis, and the potential E of the steel is expressed in mV in the x-axis. Data previously presented in Figure 1 from other sources are reproduced here as well and represented by the open gray circle symbols. The open and red circles symbols correspond to the First Stage and Second Stage C_T results, respectively, for those specimens that reached a confirmed corrosion activation condition during the duration of the tests. The results of the First Stage and Second Stage specimens that did not reach activation during the tests are indicated by the open and solid red diamonds symbols with an upward pointing arrow. The results for specimen 7 (Second Stage) are shown as a range, which were affected by added uncertainty as noted earlier.

The present findings of both experimental stages are generally consistent with the overall body of evidence, and support the expectation of a substantial increase in threshold as the impressed potential becomes more negative. The presently obtained results, considered together with those from earlier sources still support a lower bound of the beneficial effect of cathodic polarization consistent with that identified earlier, and summarized by the dashed blue line starting at E=-100 mV for C_T=0.5% and $|\beta_{CT}|$ of ~550 mV/decade of Cl^-.[5, 10] Those parameter values will consequently be used as the main base for the PDT model calculations presented later in this report. However, it is noted that several values from the present experiments and other sources are present as a lower chloride concentration bound (especially at the more negative potentials around -400 mV to -600 mV SCE). Hence, it is possible that future experiments may provide the foundation for justifying a somewhat more optimistic $|\beta_{CT}|$ slope (e.g, in the order of ~400 mV/decade of Cl^-), which may serve as a basis for more refined calculations in follow-up work.

It is also noted that the potential effect on C_T implied by Figure 15 has been figured generally on the actual concentration of chloride ions at the steel-concrete interface at the time of activation. Additional benefit could be derived from any migration effect that the electric field used to apply cathodic polarization through the concrete may have in slowing down chloride ion buildup at the steel surface.[30] For a given steel polarization level that extrinsic effect would vary depending on factors such as the electric conductivity of the concrete, and should be evaluated separately. Similarly, the cathodic reaction increases local alkalinity at the steel surface, which is expected to be a factor in elevating the effective value of the threshold.[31] The extent to which these factors may be responsible for the overall increase in threshold is likely to depend on cement composition and electrokinetic effects, and is currently being investigated in FDOT project BDV25 977-10 also for possible future refinement of model projections.

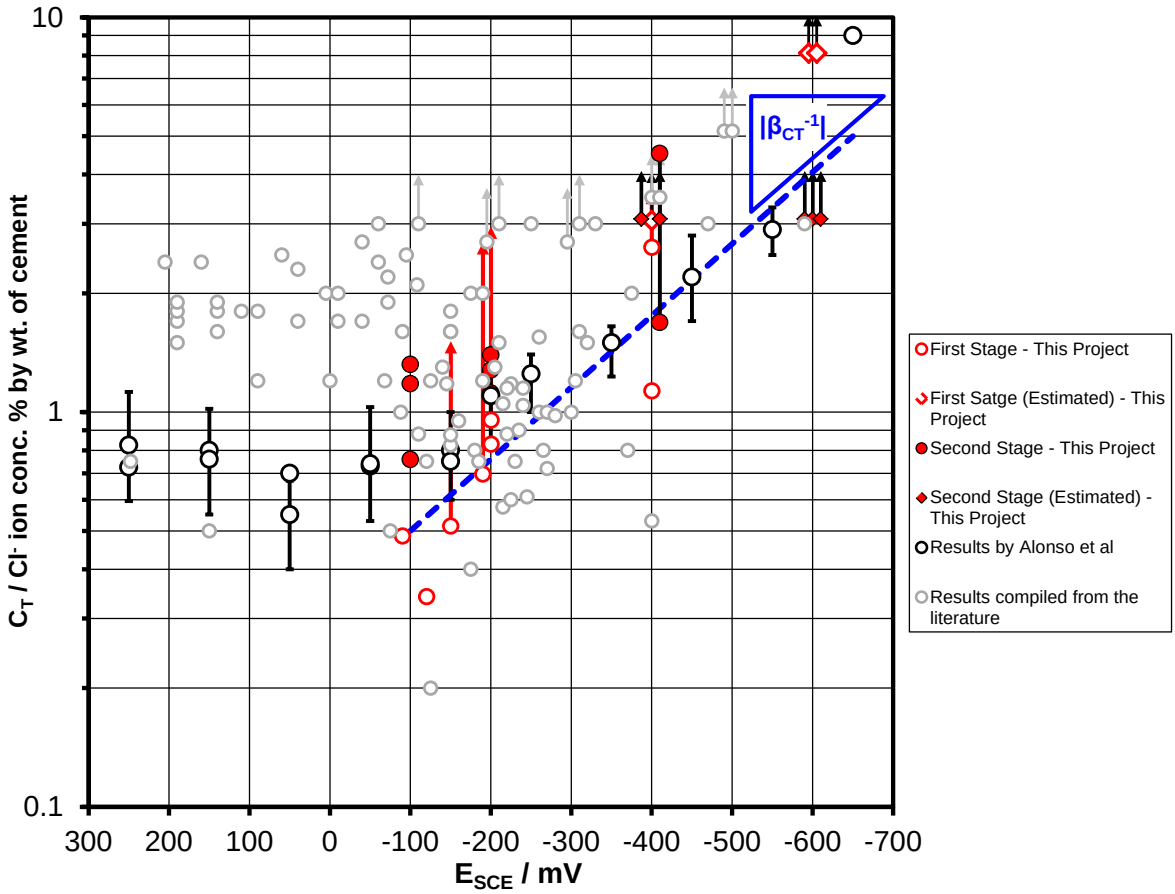

Figure 15 Chloride Threshold vs Steel Potential. Initial compilation by Presuel-Moreno et al [5]; updated by Sánchez and Sagüés (gray symbols).[6] This project: red symbols. See text for further details. Some symbols are slightly offset for clarity.

3.4 Conclusions of First Stage and Second Stage findings

- The present results tend to agree with those of previous investigations showing that negative polarization of several hundred mV may be needed to attain an increase in corrosion initiation threshold of about one order of magnitude.

- The updated survey of the literature is consistent with the lower bound of that beneficial effect being approximately described by a threshold value in the order of 0.5% by weight of cement at E=-100 mV (SCE), with a $|\beta_{CT}|$ of ~550 mV/decade of Cl^- (dashed blue line in Figure 15) of chloride content, possibly revisable to a less pronounced value. Extrinsic effects, such as an electro kinetic slowdown of chloride buildup at the steel upon cathodic polarization will require separate consideration in follow-up work.

- Because of the nature of lower bound estimates with high C_T values at the more negative potentials, and per the other considerations noted above, the use of a more optimistic slope (e.g. $|\beta_{CT}|$ = ~400 mV) may merit future consideration but in the meanwhile the value of -550 mV has been adopted for general use in the models detailed later in this report.

4 MODELING IMPLEMENTATION

4.1 Overview of model development and products

The model development took place generally in response to the project objectives outlined in Section 1.2. A probabilistic corrosion damage projection was implemented (Section 4.2) based on the modeling approach created in earlier FDOT development work. [32] Individual probabilistic damage projections were made for each combination of concrete type, structural element type, and exposure conditions (a Class[(2)]) present in the bridge to be analyzed. Each projection used corrosion development parameters that were assigned by the program based on the corresponding FDOT data base for each relevant combination of Classes in the bridge explained in more detail in section 4.4. Correction for dynamic evolution of corrosion threshold (section 4.3) was then applied to the output for each individual relevant Class combination. After correction, in an integrated model (Section 4.4) the damage results were multiplied by the number of elements in that Class, yielding an overall damage function for the structure as function of service age. That global outcome is then contrasted with the limit state defined by the user, to establish whether the durability design goal for a new structure (or remaining life for existing structures) is achieved or not. The program output is usable alternatively to establish whether specific portions of the structure can achieve individual goals.

4.2 Probabilistic Damage Projection

The principles of probabilistic corrosion damage projection have been described in detail elsewhere so only a brief summary is presented here.[33] Each portion of the structure of a given Class is divided into a group of multiple elements of equal surface footprint A_e. Each element has properties and environmental conditions that differ probabilistically from the group average reflecting the natural variability of those parameters. The parameters include the concrete cover X_C, chloride diffusion coefficient D, chloride surface concentration $C_{S,}$ and the corrosion threshold C_T. All those parameters and their variability are considered to be time-independent. In particular, the C_T values do not vary as different elements become active, so the provisional calculations deal with potential-independent threshold (PIT) values for that parameter. The model then proceeds to calculate the time t_i for corrosion initiation of each element (which varies from element to element depending on the particular values given to it by the probabilistic function assumed), adds to each a globally assumed value of the length of the propagation stage t_p, and reports as $t_s = t_i+t_p$, the time for damage declaration of that element. The fraction of the total number of elements that by an age t satisfy the condition $t_s < t$ is the value of the provisional damage function (PDF) for that Class.

As detailed in Ref [33] from which part of the following is extracted, t_s for a given element in a Class may be viewed as a function of parameters such as X_C, D, C_S, C_T, etc.:

$$t_s = f(X_C, D, C_S, C_T \dots) \qquad \text{Eq.(5)}$$

If the values of all the parameters other than X_C were kept the same, then the value $X_{C'}$ of X_C that results in damage appearing at time $t_s \leq t_p$ could be expressed as a function of the other parameters such as:

[(2)] Not to be confused with a concrete class, which is identified in the following by inserting the word "concrete" first.

$$X_{C'} = f(t_s, D, C_S, C_T \ldots) \quad \text{Eq.(6)}$$

For generality, a series of variables $X_C, V_2 \ldots V_n$ can be considered where $V_2, \ldots, V_n$ represent all the relevant factors other than X_C. Thus a more general form of Eqs. (5) and (6) is:

$$t_s = f(X_{C'}, V_2, \ldots, V_n) \quad \text{Eq.(7)}$$

$$X_{C'} = f(t_s, V_2, \ldots, V_n) \quad \text{Eq.(8)}$$

In an actual structure these parameters are subject to variability that can be both systematic (for example changes with elevation) and probabilistic (such as changes in batch-to-batch of concrete). It will be assumed that the structure can be divided into separate Classes such that within each range the values of variables $X_{C'}$, $V_2 \ldots V_n$ obey independent probability distributions. In the following, Classes will be numbered 1,2,...i....N_r, and elements within each region will be numbered 1,2,...j...N_i.

Calling P_{ki} the probability distribution function for variable V_k in region i and $P_{cum1i}(X_{Cs})$, the cumulative probability for X_{Cs}, the PDF takes the form

$$Nd(t)/N = (1/\sum_i N_i) \sum_i N_i \int_{V2} \cdots \int_{Vn} P_{cum1i}(F(t, V_2, .. V_n))\, P_{2i}(V_2) \ldots P_{ni}(V_n)\, dV_2 \ldots dV_n \quad \text{Eq.(6)}$$

where Nd(t) is the number of elements in the entire bridge reaching damage declaration at age t, N is the total number of elements in the bridge, and N_i is the number of element in Class i.

For the model implementation addressed in this report, the relevant variables have been chosen as $V_2 = C_S$; $V_3 = D$; $V_4 = C_T$; $V_5 = t_p$, of which only X_C, V_2 and V_3 are distributed while V_4 and V_5 are constants within each Class. Variability in C_T, however will be implemented explicitly subsequently via the dynamic evolution models, and implicitly via variability in C_S as noted later (Section 4.4). Because in the cases of interest t_p tends to be small compared with t_i, variability in t_p will not be addressed but that choice is deemed to be of little impact on the model output. Assuming simple Fickian chloride diffusion, time-invariant chloride diffusion coefficient and surface concentration results in t_s being given by

$$ts = \frac{x^2}{4D\left(\text{erf}^{-1}\left(1 - \frac{C_T}{C_S}\right)\right)^2} + tp \quad \text{Eq.(7)}$$

and

$$\frac{Nd(t)}{N} = \frac{1}{\sum_i N_i} \sum_i N_i \int_{Dli}^{Dhi} \int_{Csli}^{Cshi} P_{cumxi}\left(2\sqrt{D(t - tp_i)}\,\text{erf}^{-1}\left(1 - \frac{C_T}{C_S}\right)\right) P_{csi}(Cs)\, P_{Di}(D)\, dCs\, dD \quad \text{Eq.(8)}$$

where Dl_i, C_Sl_i and Dh_i, C_Sh_i represent the lowest and highest values, respectively, of D and C_S, in Class i. The total projected damaged surface area S(t) in the substructure at age t is then:

$$S(t) = Nd(t) \cdot A_e \qquad \text{Eq.(9)}$$

The choice of parameters defining the probability distributions of X_C, C_S and D as well as the integration limits for each Class is addressed in Section 4.4.

4.3 Dynamic computation (PDT and PIT combined modeling)

4.3.1 Principles of dynamic modeling to account for threshold updating.

Many of the durability models available, including that described in Section 4.2, assume a system with time-invariant C_T. However, as shown in Section 2, there is increasing evidence that C_T varies with potential of the passive steel as indicated in Eq. (1). A recent deterministic computational model developed during this project and earlier FDOT-sponsored research incorporated a potential-dependent-threshold (PDT) per Eq. (1) in an innovative damage estimation approach that integrates the initiation and propagation stage in a single model.[3, 4] The model updates the macrocell current and potential distribution of the system as new regions of the reinforcing steel assembly become active, and determines how C_T evolves in the still passive regions, adjusting the timing of subsequent corrosion initiation events accordingly. In that previous work, the model was implemented for a marine reinforced concrete column partially submerged in seawater with an invariant chloride diffusion coefficient D and concrete cover X_C. The C_S, concrete resistivity ρ, and oxygen diffusion coefficient DO_2 profiles varied systematically and uniformly with elevation, following typical marine service trends. Cases where C_T was independent of E were also modelled for comparative purposes. The concrete deterioration was quantified as a damage function of time. The cases with PDT resulted in a dramatically reduced damage projection at long service times, compared to output from the time-invariant C_T cases, highlighting the importance of considering PDT in a damage-prediction model. Those introductory calculations were deterministic, with systematic but not random variation of key parameters.

The system chosen for simulation consists of a cylindrical reinforced concrete structure exposed to a marine environment and submerged to half its length L. It has a column diameter Φ, concrete cover X_C where the rebar mat is located. The following system description is identical to the one discussed in previous work. [3, 4] For simplicity, an idealized one-dimensional model was used here to represent the column, comparable to that employed by the authors in related work. As shown there, that approach captures most of the features of interest of the system with minimum computational burden. The rebar mat, treated as a uniform sheet, has a total surface area of steel exposed to concrete equal to the external lateral column surface area multiplied by a Steel Factor S_F. The ends of the cylindrical column are considered to be isolated electrically and from the surrounding environment, and with no reinforcement.

The column is assumed to be immersed in seawater to half its length. The concrete is approximated as an effectively homogeneous electrolytic medium of resistivity ρ, effective chloride ion diffusion coefficient D, and effective oxygen diffusion coefficient DO_2 all of which are functions of elevation. Concrete on the lateral surface of the column is assumed to have developed very early a time-invariant chloride ion concentration C_S that is a function of elevation, and a time-invariant effective oxygen concentration C_{SO} treated as being constant with elevation.

The reinforcing steel is assumed to be the locus of an anodic metal loss reaction as shown in Equation (13):

$$Fe \rightarrow Fe^{+2} + 2e^{-} \quad \text{Eq.(10)}$$

with a corresponding current density i_a, under two modalities: passive dissolution at a fixed small current density i_p, or active dissolution at a potential-dependent current density i_{aa} so that Equation (14a):

$$i_a = i_p \quad \text{(passive state)} \quad \text{Eq.(11a)}$$

and Equation (14b):

$$i_a = i_{aa} = i_{o_a} 10^{\left(\frac{E - E0a}{\beta a}\right)} \text{ (active state)} \quad \text{Eq.(14b)}$$

where i_{0a} is the nominal exchange current density, E_{0a} is the nominal equilibrium potential and β_a is the anodic Tafel slope. The steel is also assumed to support a single cathodic reaction, oxygen reduction, Equation (15):

$$O_2 + 2H_2O + 4e^{-} \rightarrow 4OH^{-} \quad \text{Eq.(12)}$$

which is considered for simplicity to occur under either a fully activation-controlled or a fully diffusion-limited conditions. Under fully activation control, the current density is

$$\boldsymbol{i_{ca} = i_c = i_{o_c} 10^{\left(\frac{Eoc - E}{\beta c}\right)}} \quad \text{Eq.(13)}$$

where i_{0c} is the nominal exchange current density, E_{0c} is the nominal equilibrium potential, and β_c is the cathodic Tafel slope. Under full diffusional control, the current density is: Equation (17):

$$\boldsymbol{i_{cd} = i_c = \frac{4FDC_{SO}D_o}{X_c S_F}} \quad \text{Eq.(14)}$$

where 4 is the number of electrons to reduce O_2, F = 96.5 × 10^3 C/equiv is Faraday's constant, C_{SO} is the oxygen concentration in the pore water at the external concrete surface, and DO_2 is the effective diffusion coefficient of O_2 in the concrete, scaled to match the concentration units used. The value of i_c is made to switch from i_{ca} to i_{cd} when the former exceeds the latter, creating a working approximation in lieu of the more computationally mixed polarization function. [34]

As indicated in previous publications [3, 4], the model computes the accumulation of chloride at the steel surface with time and declares elements active as the local value of C_T is exceeded. The corrosion propagation stage is addressed by computing the increasing amount of steel loss and declaring a given segment as damaged when a critical corrosion penetration amount is exceeded. Those features of the model are addressed in detail in the previous publications and will not be further treated here. Calling x the distance along the column axis and defining and treating the problem as one-dimensional in a manner similar to that used in Ref. [12] the charge conservation condition implies that Equation (18):

$$i_s = \left(\frac{\emptyset}{4\, S_F}\right)\left(\frac{1}{\rho}\frac{d^2E}{dx^2} + \frac{d\rho^{-1}}{dx}\frac{dE}{dx}\right) \quad \text{Eq.(15)}$$

where $i_s = i_a - i_c$ is the net current density on the steel surface at elevation x , with i_a being equal to i_{aa} or i_p depending on whether the local steel surface was declared active or passive if the value of C was above or below the value of C_T, respectively.

Solution of Eq. (18) to obtain i_S and E as function of x is conducted iteratively for each time t using finite differences on a 101-node equispaced array along the elevation direction. The declaration of whether a given node corresponds to active or passive steel is made using the value of chloride concentration predicted by solution of Fick's 2nd law (as indicated in the previous papers [3, 4]), and the local value of C_T calculated at each node per Eq.(1) from the value of E obtained at the end of the iterations conducted in the previous time step. The array of values of C_T remains unchanged during the iteration process. After iteration is complete the potential array is used as seed for the next time step potential calculations. It is noted that once steel at a given node is declared active, it remains so for all subsequent time steps. This is only a simplifying assumption that may be refined in future implementations of the modeling concept.

A representative example of the model output is shown in Figure 2, where the corrosion damage projection exhibits that introduction of PDT in the model can dramatically reduce the amount of projected damage in the aged structure, compared to the output of traditional PIT modeling approaches that neglected PDT. However, as mentioned in section 2.1.1 the concrete surface damage projection was sensitive to the size of the activation zone (or node). Further correction for the local solution resistance in associated with geometric current constriction in the immediate neighborhood of the rebar was developed under this project and the approach has been published elsewhere [35, 36], hence, it is not repeated here. This treatment effectively resolved the modeling issue on sensitivity of the result to the choice of the activation zone size, which had been noted in Chapter 2.

4.3.1.1 Cases examined

These cases examine the response of the output of the model refined under this project to changes in input variables. Two general schemes (Scheme 1 and Scheme 2) were examined for variation of exposure and concrete parameters with elevation. All cases were computed with a $|\beta_{CT}|$ value of ~550 mV/decade of Cl^-, based on the experimental results of this project. Cases with PIT ($\beta_{CT} = \infty$) were also modelled for comparative purposes.

In Scheme 1, the partially submerged reinforced concrete column system was used with elevation profiles of C_S, DO_2 and ρ that followed deterministic trends as those indicated in Figure 16, with parameters and variations (for DO_2 and ρ) listed in Table 3. The values of D and X_C were kept constant throughout the numerical simulation. Scheme 1 was used extensively to obtain insight on the conditions and outputs of interest.

The system modelled in Scheme 2 is comparable to that simulated in Scheme 1 but only the atmospheric portion of the column was considered, as illustrated in Figure 17.[37] The column ends were assumed to be electrically isolated and with a C_S of 0 kg/m^2. Random pattern profiles (as shown in Figure 17) were implemented for the chloride surface concentration C_S and the concrete cover X_C without the systematic overall trends that were assumed in Scheme 1. The C_S and X_C profiles were created using a random number generator and modified to minimize short wavelengths variations. Typical average values found in Florida marine structures [33], and somewhat exaggerated values of standard deviations to better reveal any possible effects from variability, were assigned to each profile and are listed in Table 4. Random variability was limited to the values of C_S and X_C. In two

case classes only one of each respectively was assigned variability, and in another case class both varied simultaneously.

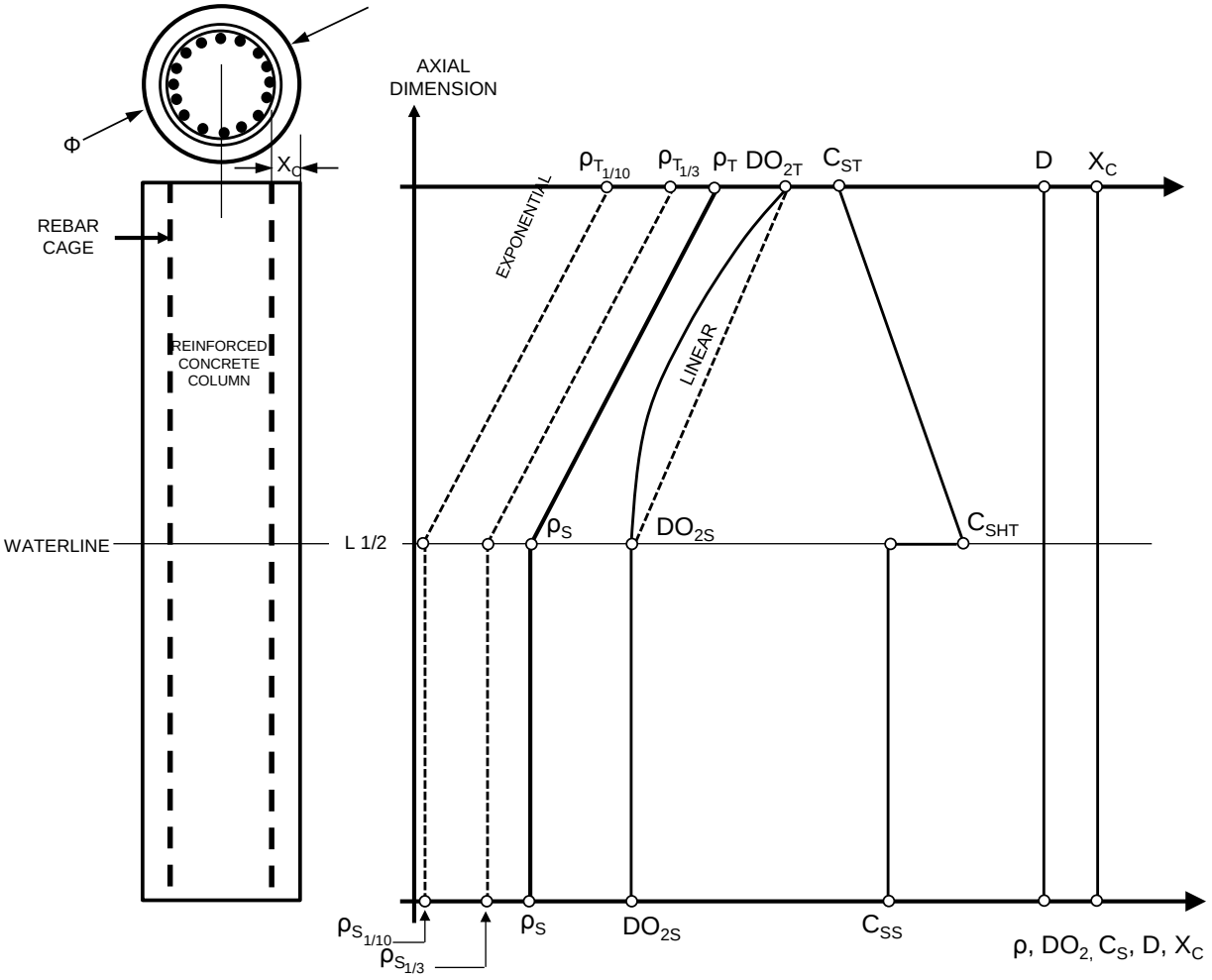

Figure 16 System modeled – Scheme 1: systematic variation of parameters.

Table 3 Model parameters for the deterministic mathematical approach (Scheme 1)

Steel Cover	X_C =	7.5 cm
Column diameter	Φ=	105 cm
Column Length	L=	1,200 cm
Concrete Resistivity	ρ_T=	2×10^5 ohm-cm (Base); ×1/3, 1/10 (Variations)
	ρ_S=	4×10^4 ohm-cm (Base); ×1/3, 1/10 (Variations)
Oxygen diffusion coefficient	DO_{2T}=	10^{-3} cm^2/s
	DO_{2S}=	10^{-5} cm^2/s
		Log D varies linearly with elevation (Base)
		D varies linearly with elevation (Variation)
Chloride diffusion coefficient	D=	2.5×10^{-8} cm^2/s
O_2 Surface Concentration	C_{SO}=	2.5×10^{-7} mol/cm^3 (in pore water)
Cl^- Surface Concentration	C_{ST}=	0 kg/m^3
	C_{SHT}=	20 kg/m^3
	C_{SS}=	9 kg/m^3
Chloride Threshold Parameters	C_{T0}=	1.78 kg/m^3
	E_{T0}=	-100 mV
	β_{CT} =	550 mV/decade of Cl^- (Base);

Polarization Parameters**	E_0 (-mV SCE)	i_0 (A/cm^2)	Tafel Slope (mV)
Iron Dissolution	-780	1.875×10^{-8}	60
Oxygen Reduction	160	6.25×10^{-10}	160

Steel Passive Current Density	$i_p = 0.058 \times 10^{-6}$ A/cm^2
Critical Corrosion Penetration	P_{CRIT} = 0.01 cm

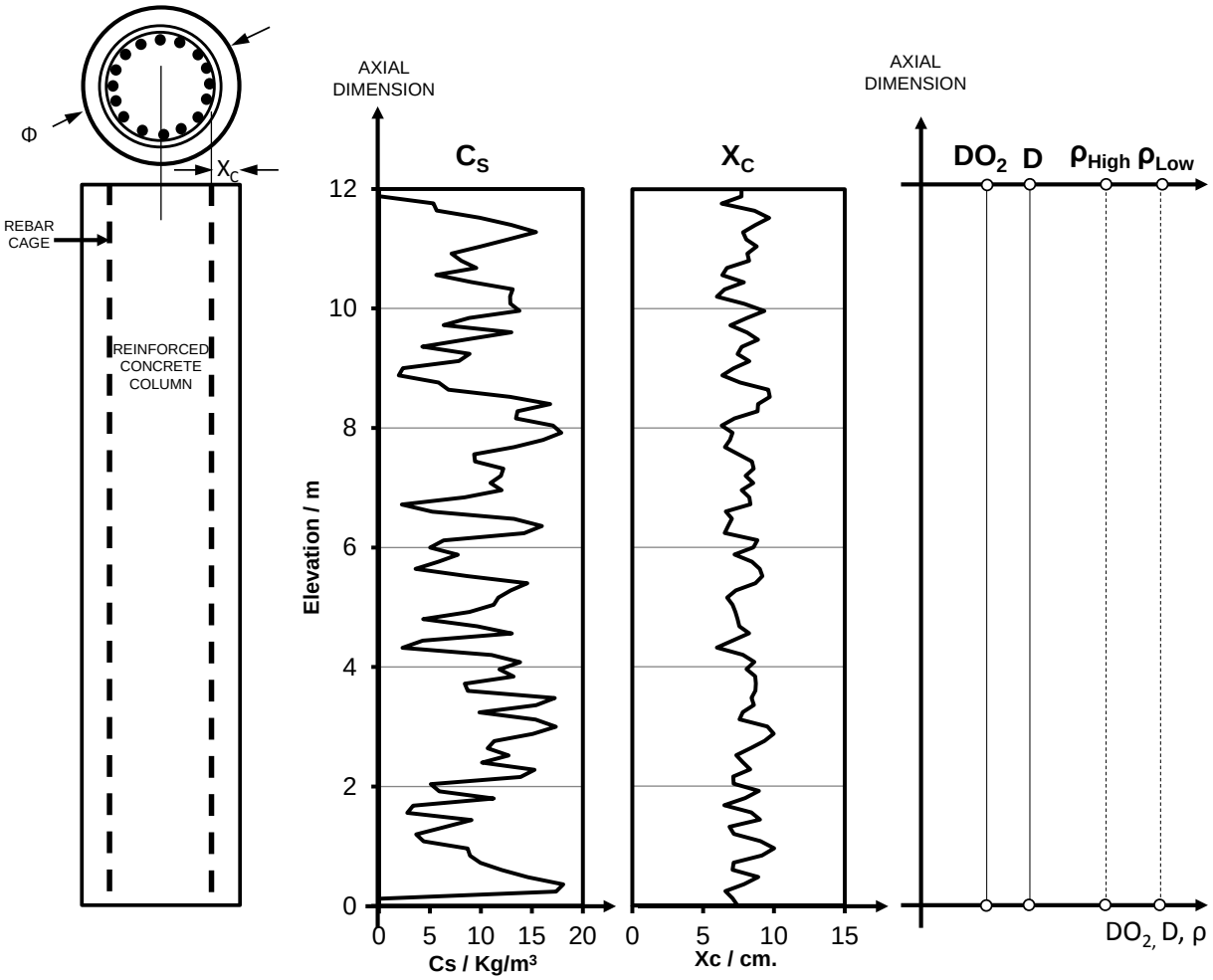

Figure 17 System modeled – Scheme 2: representative randomly distributed profiles for the surface concentration and concrete cover.

Table 4 Model parameters for the randomly distributed mathematical approach (Scheme 2)

Column diameter	Φ=	105 cm	
Column Length	L=	1,200 cm	
Steel Cover (average)	X_{Cavg} =	8 cm	
Steel Cover (standard deviation)	X_{Cstd} =	2 cm	
Cl^- Surface Conc. (average)	C_{Savg}=	10.4 kg/m^3	
Cl^- Surface Conc.(standard deviation)	C_{Sstd}=	4.5 kg/m^3	
Concrete Resistivity	ρ_{High}=	7.5×10^4 ohm-cm	(Base); ×1/3, 1/10 (Variations)
	ρ_{Low}=	1.5×10^4 ohm-cm	(Base); ×1/3, 1/10 (Variations)
Oxygen diffusion coefficient	DO_2=	2.5×10^{-5} cm^2/s	
Chloride diffusion coefficient	D=	2.5×10^{-8} cm^2/s	
O_2 Surface Concentration	C_{SO}=	2.5×10^{-7} mol/cm^3 (in pore water)	
Chloride Threshold Parameters			
	C_{T0}=	1.78 kg/m^3	
	E_{T0}=	-100 mV	
	β_{CT} =	550 mV/decade of Cl^-	
Polarization Parameters	E_0 (-mV SCE)	i_0 (A/cm^2)	Tafel Slope (mV)
Iron Dissolution	-780	1.875×10^{-8}	60
Oxygen Reduction	160	6.25×10^{-10}	160
Steel Passive Current Density	i_p= 0.058×10^{-6} A/cm^2		
Critical Corrosion Penetration	P_{CRIT}= 0.01 cm		

4.3.2 Integration of Dynamic and Probabilistic Modeling

4.3.2.1 Overall approach

The information developed from experimental measurements of the dependence of C_T on steel potential (Sections 3.1 to 3.2), and from the findings of the dynamic computer models that were built using the experimental results on PDT and combined Initiation-Propagation computations (Section 4.3.1.1), was employed to refine the output of the main damage prediction model produced by this project.

The modeling approach used was to organize the functioning of the main model in the following steps:

1) Conduct a provisional probabilistic damage projection for a Class. This is done following the overall procedure described in Section 4.2, which assumes PIT conditions.
2) Apply a correction to the preliminary damage function (PDF), calculated for PIT conditions in the previous step, to account for PDT and obtain the final program output damage function (DF). The correction approach is used instead of a direct model because PDT calculations are highly computer-resource intensive and direct

incorporation into a probabilistic model is deemed to be impractical at present. The approach was developed in the following manner:

a. Computed separate simplified PDT calculations that have been made for a number of scenarios that capture the main characteristics of marine substructure conditions (those presented in section 4.3.1.1), and a similar set of calculations was made with the same systems, but assuming PIT conditions instead.

b. Comparison of the PDT and PIT results was then made to formulate a correction function that, when applied to the PDF obtained under PIT, results in a suitable approximation of the corresponding PDT scenario. The correction function was developed as a global abstraction from the result of computing a representative collection of the cases of interest.

The global correction function is then applied to the PDF obtained in the previous step. The result is the DF that constitutes the final output of the predictive model for that Class. The output thus corrected for all Classes is then tallied to obtain the damage function for the entire system, or for selected parts as desired. .

The next section describes how the correction function was developed and the formulation adopted.

4.3.2.2 Correction function

The basic scenario to develop the correction function was the generic reinforced concrete column system already described in section 4.3.1. Representative examples of the comparative output of the scenarios explored of Scheme 1 (systematic parameter distributions, systematic resistivity variations) and Scheme 2 (random X_C, random C_S and combined random profile) are shown in Figure 18 and in Figure 19, respectively.

As noted earlier, a dominant trend of significantly lower amount of long term damage for PDT compared with PIT was observed in these as well as all the other variations examined. Examination of the shape and magnitude of the damage functions calculated for PDT-PIT pair combinations from the Table 3 and Table 4 cases showed that the long term (75 year) ratio of PIT to PDT damage percent ranged from ~2 to ~5. For the purposes of practical implementation of this effect, a value of 3 is proposed as being representative of a long term correction ratio C_{LTR}. It is noted that the behavior differentiation described here as taking place in the long term is actually for an extended but intermediate time period, when chloride levels at the steel depth are substantial, but have not yet became so high so as to exceed the chloride threshold at the zones of greatest potential depression. At very long structure ages, and if the surface chloride concentration is high enough, the amount of damage in the PDT case may eventually approach the terminal amount of damage for the comparable PIT situation. Hence, the concept of a long term ratio, and the representative value adopted for it are to be considered as working approximations subject to update and refinement in future investigations.

At lower ages and lower levels of damage (e.g. a few %) the manifestations of early damage for PDT and PIT tended to appear at comparable times but with some variability, with one or the other taking the lead by a few years over the other. Instances where PDT took the lead at early damage levels appeared to be more evident in cases where the system parameters were subject to random variations as shown in Figure 19, and less so when systematic changes with elevation dominated. As noted elsewhere [37] the instances where PDT takes

the lead may be explained as being the result of a propagation stage phenomenon and, paradoxically, a result of the delay in other activation events following the first ones. That delay enables sustained macrocell enhancement of the relatively few early active regions with consequent faster local corrosion rates for those few regions, causing their early declarations of damage. In contrast, for PIT the rate of appearance of new active regions is not decreased and thus the remaining cathodic portion of the steel assembly has to support an increasing number of anodes, with consequent less enhancement of the corrosion rate in those anodes and slower onset of the damage declarations. It is noted that these simulations have been conducted with parameter choices that tended to result in relatively short times to corrosion initiation, in order to reduce the need for long computational runs while still spanning a large range of total damage development. Hence, the calculations tended to emphasize any effect of propagation period-related differentiation such as the one just discussed. That type of effect is expected to be relatively modest in the overall service life estimate for the structures commonly designed by FDOT (many decades), where highly impermeable concrete is often specified if the environment is aggressive. The chloride diffusion coefficients are small in those cases and consequently the initiation stage is the dominant period in the service life of the structure and propagation stage-related phenomena tend to be less important. Hence, pending detailed examination in follow-up research, the differentiation between PDT and PIT cases in the early stages of damage is treated here as being of secondary importance. Based on the above and on the results of the simulations conducted, a working approximation is proposed whereby the damage projection for PDT conditions was considered to be the same as that for PIT conditions up to a nominal crossover value C_{CR} = 2%. Further refinement of that value and of its underlying concept is pending on future investigations.

Per the above considerations and for the purposes of the durability model formulation delivered under this project and described in Appendix 1, adjustable provisional nominal values for the long-term correction ratio C_{LTR} = 3, and for the crossover damage percent C_{CR}= 2 % were adopted. For the entire service life forecast then the corrected damage function DF is obtained from the preliminary damage function PDF by:

$$DF = PDF(t) * \gamma(PDF(t)) \qquad \text{Eq.(19)}$$

with the PDT Partial Factor γ defined by:

$$\gamma = 1 \qquad \text{for PDF(t)} < C_{CR} \qquad \text{Eq.(20)}$$

$$\gamma = \frac{1}{1+(C_{LTR}-1)\cdot\frac{PDF(t)-C_{CR}}{100\%-C_{CR}}} \qquad \text{for PDF(t)} \geq C_{CR} \qquad \text{Eq.(21)}$$

Reflecting the previous discussions, at long ages when PDF approaches 100% in severe environmental exposures, γ approaches $1/C_{LTR}$. At short ages the value of γ becomes increasingly close to unity while approaching the crossover early regime.

Equation 21 presupposes that within a given Class the exposure conditions are severe enough that given a sufficiently long service time, the PDF would reach nearly 100% damage. It also presupposes that the distribution of times to damage declaration within the Class is not distinctly multimodal. It should be noted that in the Scheme 1 cases the damage evolution was indeed bimodal (with strong above- and below-water differentiation). In that

case, the long term damage for the above-water portion dominated during much of time interval investigated, so apparent terminal damage was 50% instead of 100%, and the value of C_{LTR} was evaluated via the PIT-PDT damage ratio during that domain. Clearly for distinctly multimodal cases application of Eq. (21) would only serve as a rough approximation. For the general intent of the modeling approach proposed here, where conditions within individual Classes tend to be somewhat regular, Eq. (21) represents a working compromise pending the development of more sophisticated approaches in the future.

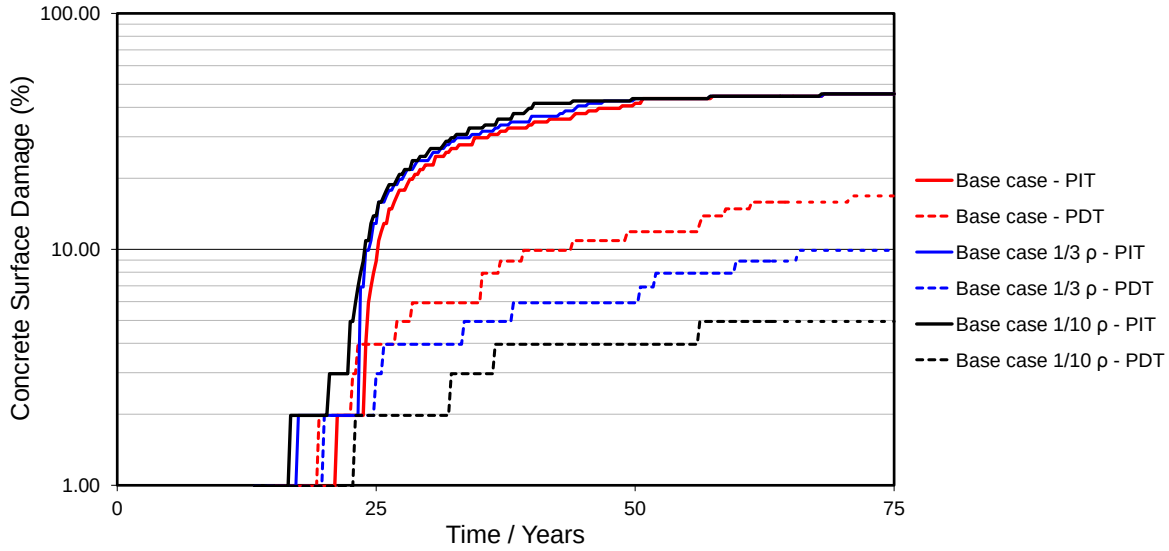

Figure 18 Example of comparative PIT-PDT output for Scheme 1 cases where resistivity at each elevation level was varied from the base case by multiplication factors of 1, 1/3 and 1/10.

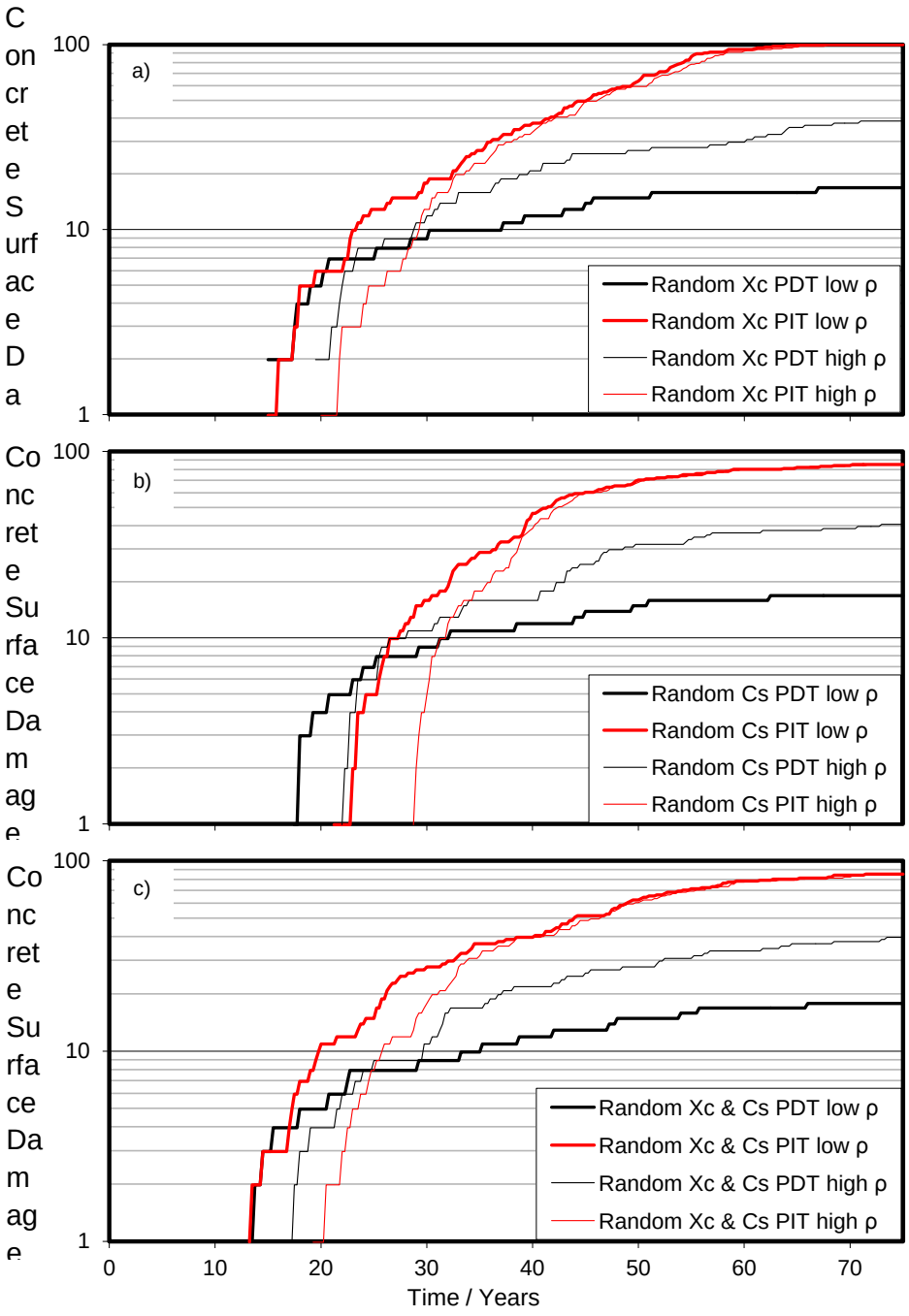

Figure 19 Example of comparative PIT-PDT for Scheme 2 cases. a) Randomly distributed X_C. b) Randomly distributed C_S. c) Combined case

4.4 Integrated Predictive Model

The Integrated Predictive Model is the main product of this project. An alpha version of this model is provided to FDOT as a separate deliverable. That version serves as a working prototype for evaluation and subsequent adaptation by FDOT into user-compatible platforms that may include versions for internal FDOT use, and versions for incorporation in the Structures Design Manual and related documentation for a broader audience. Internal default values for parameters in the alpha model include provisional entries (see Table 5) that are updatable as new information or improved interpretation of existing data becomes available. Hence, eventual use of the model for decision making purposes is contingent on subsequent finalized adoption of an appropriate set of parameter values as well as updated simplifying assumptions as needed. A picture of the user interface with program output and user instructions is presented in Appendix 1.

The model receives user input on the makeup of a bridge substructure (highest corrosion risk region) including for each type of component, the structural configuration, materials of construction and service environment, and develops an output consisting of the corrosion-related damage function for a period of 100 years for each Class of structural/environmental combinations and for the structure as a whole. The following functionalities are incorporated:

Structural components: In its present version the program considers three types of structural components: square piles, rectangular footings, and round columns, each having type-specific external dimensions and steel clear cover. The clear cover can be either as prescribed by the SDG according to the environmental classification of the service environment (see next item), or user-selected if the effect of variations from prescribed values is to be explored. The rebar size is selectable as well. Based on the type and size of the component, a fraction of its surface is assigned to one of four chloride penetration regimes: flat wall, 2-way corner, 3-way corner and round.[38] For square piles of side dimension Y the perimeter of the cross section is 4Y, of which a fraction $8*(X_C)$ /4Y (where X_C is the steel cover) is deemed to correspond to the length of the perimeter representative of a 2-way corner exposure geometry, and the rest $(4Y-8*(X_C))$ /4Y to the flat wall exposure geometry. A comparable assignment based on rebar cover and dimensions is made for the parallelepiped footing geometry to assign fractions representative of flat wall, 2-way and 3-way corners. For round columns, the entire surface is assigned a round condition.

Exposure conditions: Each component type can be distributed (by specifying number of components in each) into two main types of exposure conditions: in water (IW), and in soil (IS). For the IW type there are 4 sub-exposure types: submerged near surface, tidal zone, splash-evaporation, and atmospheric (S, T, SE and A, respectively). The program does not require user entry for the total absolute elevation range at-corrosion-risk, which has been internally set at 16 ft starting 2 ft below the bottom of the T condition region, as a placeholder to represent typical conditions in marine substructure. However, user input for that range size as well as for the fraction assignations given next can be easily implemented in new model versions if desired. The sub-exposure type fractions of the total elevation range are assigned as 1/8, 1/8, 3/8 and 3/8 of the total for S, T, SE and A, respectively. Square piles and columns are assumed to be of uniform cross section and exposed laterally to the entire range, so the corresponding at-corrosion-risk area fractions are given by the same values. Footings are assumed to be exposed only to the S,T and SE regimes, laterally as well as on the top surface for the SE regime, with the corresponding surface area fractions calculated accordingly by simple geometry.

For the IS type there are two sub-exposures types: buried and atmospheric (B and A, respectively), each spanning a nominal height of 8 ft for piles and columns and assigning each ½ of the at-risk area. For the footings the B and A elevation ranges are assumed to be 5 ft each, with area fractions obtained by appropriate calculations. More complicated structural member geometries, including for example columns on top of footings can be incorporated for each of the exposure condition types at the discretion of the Florida Department of Transportation following the same procedures.

For the IW and IS components, three environmental classifications (Extremely Aggressive, Moderately Aggressive and Slightly Aggressive) can be selected by the user. By selecting an environmental aggressiveness, default values for the chloride concentration in water, chloride concentration in soil, and concrete cover are assigned in accordance to the SDG. Those default values can be modified by the user as well.

Concrete properties: Each component type is assigned an FDOT concrete class[(3)] ranging from concrete Class I to concrete Class VI. In the present model implementation, for simplified generic calculations each concrete class is assigned a time- and space-invariant value of chloride ion diffusion coefficient, with a baseline provisionally abstracted from the present body of properties information from FDOT reports and related data. The baseline values for the concrete classes are listed in Table 5. As a first alternative to default values, user-selected values of the diffusion coefficient can be directly entered in the worksheet to replace the baseline value. As a second alternative, the user can have the program obtain an estimate of the diffusion coefficient based on concrete cement factor, percentage of pozzolanic or slag cement replacement and water-to cement ratio. The calculation is performed using the relationship developed under FDOT project BA502 [39] to estimate concrete chloride diffusion coefficients, based on regression of field data from a group of bridges about 10-years old and built with modern concrete formulations. That estimate is best applicable to the higher concrete class types.

Once the diffusion coefficient is set, a multiplier is assigned based on the ratio of rebar diameter Φ_r to concrete cover X_C to reflect the increased rate of chloride accumulation due to the obstruction presented by the rebar. The value of that multiplier ($1/Tf$), related to the ratios of Φ/X_C and the C_T/C_S, has been abstracted from work developed in prior FDOT projects assuming a flat wall regime with the presence of a single rebar. [22, 23] Additionally, the value of the chloride diffusion coefficient is further conditioned (to obtain a fictitious equivalent value) by adopting a multiplying factor to correct for the geometric regime effects (2-way corner, 3-way corner and round) based on characteristic correction factors developed in an earlier FDOT project.[38] For the case of the round columns, the factor is a function of the ratio C_T/C_S and the ratio of the radius r of the column to concrete cover X_{Cobs} corrected for the rebar obstruction effect. Reference [39] reported values only for X_{Cobs}/r = to 0.1, 0.2, and 0.3; therefore the correction in the present version is constrained to those values. Cases with X_{Cobs}/r values less than 0.1 or greater than 0.3, are approximated as having a value of 0.1 or 0.3, respectively. All these geometric adjustments are slated for more refined treatment in future versions of the model.

The same FDOT project that developed a T*f* adjustment to correct for rebar presence in a flat wall also investigated the case of a 2-way corner with a single rebar presence.[23, 38, 39] Results were comparable with those obtained assuming a 2-way corner geometry without correction for rebar obstruction effect, likely because the corner geometry already

(3) Not to be confused with a structural/environmental Class for damage projection calculations; see footnote 2.

incorporated a strong multi-dimensional aggravation of chloride ingress. Therefore, in the present model chloride penetration in a 2-way corner geometry regime was not adjusted for rebar presence. For the case of a 3-way corner there is no available information at present on the effect of rebar presence, but by analogy with the 2-way case no correction for rebar presence was made in this situation either, it is suggested that the rebar presence effect in 3-way corner geometry should be examined in follow-up investigations.

Following practice from previous probabilistic model realizations in FDOT-sponsored modeling efforts, the chloride diffusion coefficient distribution was represented by a normal distribution with an average value equal to the baseline after being modified for the appropriate adaptations indicated above, and with a coefficient of variation and upper and lower limits values as listed in Table 5.

Notably, the present modeling approach does not include time-variability of the chloride diffusion coefficient, whereby some reduction in value would be projected as the structure ages.[40] That feature is not included because much on the information on chloride diffusion coefficient developed by FDOT has been obtained from cores extracted from its structures at mature ages (e.g. typically >10 years [39, 41]), in the form of effective long-term diffusion coefficient values. It is those diffusion coefficient values, rather than values extrapolated from very short term laboratory tests, that are primarily intended to be used in the model developed under this project. This choice of time-independent diffusion coefficient is somewhat conservative, especially for concrete with pozzolanic and slag additions where the most pronounced further decreases in the diffusion coefficient might be expected as a structure ages [2, 40, 42]. However, it is noted that scarcity of long term data introduces uncertainty in the validity of expecting a sustained decline in diffusion coefficient in the long term. Indeed, in the Life-365 program [2]credit for beneficial aging is suspended for that reason for periods beyond about 3 decades of service. Hence, the extent of conservativeness introduced by using the present approach is limited as it concerns a relatively short relative time period before other uncertainty sets in. The potential beneficial reduction in diffusion coefficient would be limited as well due to its dependence being expected to follow only a fractional power law.[2]

Nonetheless, additional features for future development have been included in the model as placeholders. These include: a) the use of the rapid chloride migration coefficient (D_{RCM}) obtained through the Nordtest NT Build 492 procedure [43] to convert it into an effective chloride diffusion coefficient, and b) the expansion to admit user input to obtain chloride diffusion coefficient based on concrete resistivity or laboratory permeability data, which can potentially be incorporated with the availability of the output just published from FDOT Project BDK79-977-02. [44] In those cases, provision to account for an age factor in the value of the chloride diffusion coefficient will be necessary in future versions of the model.

At present, the model assigns for simplicity the same chloride diffusion coefficient (representative of the more severe conditions prevalent at the lowest elevations) to all the elevations within a structural element. The resulting conservativeness may be reduced as more data documenting lower diffusion coefficients at higher elevations [39] become available, by implementing user entry for elevation-dependent values. That implementation is in principle straightforward in new model versions. Likewise, the model does not make provision for input on local average temperature. Should precise enough data on chloride diffusion coefficient variation with temperature (within the relatively limited range existing in Florida) become available, a temperature correction factor can also be included in future versions.

Surface Conditions: Each of the exposure types and sub-exposure types noted above has been assigned a specific value of C_S as listed in Table 5. Those values are provisionally abstracted from the present body of properties information from FDOT reports and related data and capture trends of decreasing chloride accumulation with elevation for evaporative regimes, and chloride concentration below water. Similar to the treatment of concrete properties, following practice from previous probabilistic model realizations in FDOT-sponsored modeling effort, the surface chloride distribution was represented by a normal distribution with a standard deviation (conservatively selected as noted below) and upper and lower limits values listed in Table 5. As an alternative, the user can enter a preferred value of C_S for each sub-exposure condition.

Chloride threshold and rebar type: For its PDF calculations described in Section 4.3.1.1, the program has plain steel (PS) as the default rebar material, and as alternatives options: galvanized steel (GS), "MMFX" (ASTM A1035) and a generic austenitic stainless steel (SS). The assumed value of C_T for PS is a value equal to 0.04% of the nominal CF of each of the concrete classes, which is listed in Table 5. For the other materials the default value of C_T is adjusted by a respective multiplier also listed on Table 5. All those values have been provisionally abstracted from the information available from FDOT previous investigations and other literature sources, but are included primarily as placeholders for future development and do not constitute an endorsement of specific products and materials. The defaults can be overridden by the user if alternative scenarios are to be explored. Variability in C_T for the PDF calculation is implemented implicitly to some degree via the amount of variability conservatively assumed for C_S, since the time to corrosion initiation is not a function of C_T by itself but, per Eq.(10), of the ratio C_T/C_S, so variability in C_S results in variability in the ratio even if C_T is constant. The program introduced additional, time-variable dispersion in C_T via the subsequent conversion of the PDF into the PF by the procedures described in Section 4.3.1.

Propagation time: A default flat value of 5 years has been assigned to the value of propagation time tp, representative of the choice used in previous FDOT projects for the development of predictive models, and per the arguments for limited need to capture variability of this parameter. However, the default can be overridden by the user if alternative scenarios are to be explored, especially for the case of SS rebar, where there are indications in the literature that much longer corrosion propagation times may develop.[45].

Limit State: A corrosion related damage limit state of 2.3% surface damage (that may be viewed as being comparable to the limit value adopted by LNEC, an European agency [46]) has been incorporated as a default for rapid informal contrasting of results against an assumed durability goal, either for specific structural/environmental Classes or for the entire bridge. That default value is presented only as an example, as the development of a corrosion related damage limit state, which may have different values for specific Classes and a different meaning if applied to the entire structure, is an open issue to be decided by FDOT in future discussions. The default value can be overridden by the user to explore alternative scenarios.

Table 5 Concrete and steel bar properties for modeling parameters

Notice: These values are provisional selections intended primarily to establish model functionality. Subject to update and modification pending subsequent data evaluation, and decision on implementation of the program for Department use including determination of target user group and scope of program application.

Chloride Diffusion Coefficient, D						
D / in^2 y^{-1}	1	0.3	0.1	0.025	0.01	0.0075
Concrete class	I	II	III	IV	V	VI
Distribution formulation	mean μ	standard deviation sd	lower limit	upper limit		
	D	25%	3 x sd	10 x sd		
Chloride Surface Concentration, Cs						
			C_S / pcy			
Cl^- Concentration in Water / ppm:	>6000		Sq. Piles	Footings	Columns	
		Submerged	15	15	15	
		Tidal	40	40	40	
		Splash-Evap.	40	40	40	
		Atmospheric	15		15	
Cl^- Concentration in Water / ppm:	≤6000					
		Submerged	7.5	7.5	7.5	
		Tidal	20	20	20	
		Splash-Evap.	40	40	40	
		Atmospheric	10		10	
Cl^- Concentration in Soil / ppm:	>2000					
		Buried	10	10	10	
		Atmospheric	10	10	10	
Cl^- Concentration in Soil / ppm:	>2000					
		Buried	7.5	7.5	7.5	
		Atmospheric	7.5	7.5	7.5	
Distribution formulation	mean μ	standard deviation sd	lower limit	upper limit		
	C_S	25%	3 x sd	3 x sd		
Chloride Threshold, C_T						
Type of rebar	Plain Steel	Galvanized	MMFX	316L	316L-clad	-
Multiplier	1	2	4	10	10	-
Concrete class	1	2	3	4	5	6
CF / pcy	544	575	600	650	700	752
C_T / pcy	2.18	2.30	2.40	2.60	2.80	3.01

5 CONCLUSIONS

Experimental Investigations

- Shortages in experimental data to characterize the potential-dependent chloride threshold (PDT) behavior were successfully addressed by experiments with specimens in mortar and concrete and with considerably large area of exposed metal.

- The experiments on potential-dependent threshold determinations produced results consistent with the lower bound of that beneficial effect being approximately described by a threshold value in the order of 0.5% by weight of cement at E=-100 mV (SCE), with a negative slope of ~550 mV per decade of Cl^-. That bound was incorporated in the numerical predictive models used in this project. Extrinsic effects, such as an electro kinetic slowdown of chloride buildup at the steel upon cathodic polarization merit consideration in future work.

Resolution of remaining issues in implementing PDT in a dynamic program

- Exploratory calculations supported the validity of the hypothesis that as active zones become smaller their preventive throwing power would be reduced as well, resulting in the development of more numerous active zones that would make up for their individual smaller size in reaching to a finite damage terminal condition. The model improvement over the previous PDT model stems from a more realistic implementation of the local concrete resistance R_S around the reinforcing steel bars.

Next generation modeling approach

- Integration of a full probabilistic corrosion forecasting approach and a PDT feature was developed and achieved via a correction function that links both modalities. The corrosion factor was abstracted from comparative calculations using representative marine corrosion scenarios.

- A next-generation model was created incorporating advanced features that include a full probabilistic treatment of the damage prediction calculations with statistical variability in surface concentration, concrete cover, chloride diffusion coefficient, and of corrosion threshold by the PDT correction function. The model incorporates provisions for type of rebar material, as well as geometric aggravation effects from rebar presence and corners and curvature in the concrete surface. The model includes also functionality for variability in environmental aggressiveness conditions as a function of elevation above water, and for location of structural components in various environments in the same bridge.

- A model prototype was prepared as a separate deliverable for evaluation and subsequent adaptation by FDOT into user-compatible platforms that may include versions for internal FDOT use, and versions for incorporation in the Structures Design Manual and related documentation for a broader audience.

6 REFERENCES

[1] K. Tuutti, "Corrosion of Steel in Concrete", Swedish Cement and Concrete Research Institute, Stockholm, 1982.

[2] "Life-365 Service Life Prediction Model™ and Computer Program for Predicting the Service Life and Life-Cycle Costs of Reinforced Concrete Exposed to Chlorides", Produced by the Life-365 Consortium II, 2008.

[3] A. A. Sagüés, S. C. Kranc, and K. Lau, "Service Life Forecasting for Reinforced Concrete Incorporating Potential-Dependent Chloride Threshold". Paper No. 09213, presented at the NACE Corrosion 2009, Atlanta, GA. NACE International, Houston, TX., 2009.

[4] A. A. Sagüés, S. C. Kranc, and K. Lau, "Modeling of Corrosion of Steel in Concrete with Potential-Dependent Chloride Threshold". Paper No. 4006, presented at the 17th International Corrosion Congress Las Vegas, NV, 2008.

[5] F. J. Presuel-Moreno, A. A. Sagüés, and S. C. Kranc, "Steel Activation in Concrete Following Interruption of Long-Term Cathodic Polarization", *Corrosion,* vol. 61, pp. 428-436, 2005.

[6] A. N. Sánchez and A. A. Sagüés, "Chloride Threshold Dependence on Potential in Reinforced Mortar". Paper No. 1728, presented at the NACE Corrosion 2012, Salt Lake City, UT. NACE International, Houston, TX., 2012.

[7] M. Manera, Ø. Vennesland, and L. Bertolini, "Chloride Threshold for Rebar Corrosion in Concrete with Addition of Silica Fume", *Corrosion Science,* vol. 50, pp. 554-560, 2008.

[8] B. H. Oh, S. Y. Jang, and Y. S. Shin, "Experimental Investigation of the Threshold Chloride Concentration for Corrosion Initiation in Reinforced Concrete Structures", *Magazine of Concrete Research,* vol. 55, pp. 117-124, 2003.

[9] L. Bertolini, F. Bolzoni, M. Gastaldi, T. Pastore, P. Pedeferri, and E. Redaelli, "Effects of Cathodic Prevention on the Chloride Threshold for Steel Corrosion in Concrete", *Electrochimica Acta,* vol. 54, pp. 1452-1463, 2009.

[10] C. Alonso, M. Castellote, and C. Andrade, "Chloride Threshold Dependence of Pitting Potential of Reinforcements", *Electrochimica Acta,* vol. 47, pp. 3469-3481, 2002.

[11] P. Pedeferri, "Cathodic Protection and Cathodic Prevention", *Construction and Building Materials,* vol. 10, pp. 391-402, 1996.

[12] F. J. Presuel-Moreno, S. C. Kranc, and A. A. Sagüés, "Cathodic Prevention Distribution in Partially Submerged Reinforced Concrete", *Corrosion,* vol. 61, pp. 548-558, 2005.

[13] J. Bockris and A. K. N. Reddy, Volume 1: *Modern Electrochemistry: Ionics*, 2nd ed. Plenum Press, New York, 1998.

[14] L. Li and A. A. Sagüés, "Chloride Corrosion Threshold of Reinforcing Steel in Alkaline Solutions-Effect of Specimen Size", *Corrosion,* vol. 60, pp. 195-202, 2004.

[15] L. Basheer, J. Kropp, and D. J. Cleland, "Assessment of the Durability of Concrete from its Permeation Properties – a review", *Construction and Building Materials,* vol. 15, pp. 93-103, 2001.

[16] A. N. Sánchez and A. A. Sagüés, "Chloride Corrosion Threshold Dependence on Steel Potential in Reinforced Concrete". Paper No. 4118, presented at the NACE Corrosion 2014, San Antonio, TX. NACE International, Houston, TX., 2014.

[17] R. Weast, *CRC Handbook of Chemistry and Physics*, 54 ed. Chemical Rubber Company, Cleveland, 1973.

[18] A. A. Sagüés, K. Lau, and A. Accardi, "Mechanistic Issues on Corrosion Performance of Dual Polymer–Zinc Coated Rebar", Final Report FOR Gerdau – Ameristeel, 2010.

[19] P. P. Castro, A. A. Sagüés, E. I. Moreno, l. Maldonado, and J. Genesca, "Characterization of Activated Titanium Solid Reference Electrodes for Corrosion Testing of Steel in Concrete", *Corrosion,* vol. 52, pp. 609-617, 1996.

[20] FM5-516, "Florida Method of Test for Determining Low-Levels of Chloride in Concrete and Raw Materials", Florida Department of Transportation, 2009.

[21] J. Crank, *The Mathematics of Diffusion*, Second ed. Oxford University Press, Oxford, 1975.

[22] S. C. Kranc, A. A. Sagüés, and F. J. Presuel-Moreno, "Decreased Corrosion Initiation Time of Steel in Concrete due to Reinforcing Bar Obstruction of Diffusional Flow", *ACI Materials Journal,* vol. 99, pp. 51-53, 2002.

[23] S. C. Kranc and A. A. Sagüés, "Advanced Analysis of Chloride Ion Penetration Profiles in Marine Substructure", Final Report Contract No. BB-880", Florida Department of Transportation Research Center, Tallahassee, FL., 2003.

[24] Q. Yuan, C. Shi, G. De Schutter, K. Audenaert, and D. Deng, "Chloride binding of Cement-based Materials Subjected to External Chloride Environment – a review", *Construction and Building Materials,* vol. 23, pp. 1-13, 2009.

[25] M. G. Hernández, M. A. G. Izquierdo, A. Ibáñez, J. J. Anaya, and L. G. Ullate, "Porosity Estimation of Concrete by Ultrasonic NDE", *Ultrasonics,* vol. 38, pp. 531-533, 2000.

[26] T. Oshiro and S. Tanigawa, "Effect of Surface Coating on the Durability of Concrete Exposed to Marine Environment", in *Second International Conference Concrete in Marine Environment Proceedings*, St. Andrews by-the-Sea, Canada, pp. 179-198,1988.

[27] T. Luping and L.-O. Nilsson, "Rapid Determination of the Chloride Diffusivity in Concrete by Applying an Electric Field", *Materials Journal,* vol. 89, pp. 49-53, 1993.

[28] K. Takewaka and S. Mastumoto, "Quality and Cover Thickness of Concrete Based on the Estimation of Chloride Penetration in Marine Environments", in *SP109-17*. vol. 109, pp. 381-400, 1988

[29] ASTM Standard G109-07, "Standard Test Method for Determining Effects of Chemical Admixtures on Corrosion of Embedded Steel Reinforcement in Concrete Exposed to Chloride Environments", ASTM International, West Conshohocken, PA, 2007, www.astm.org

[30] N. R. Buenfeld, G. K. Glass, A. M. Hassanein, and J. Z. Zhang, "Chloride Transport in Concrete Subjected to Electric Field", *Journal of Materials in Civil Engineering,* vol. 10, pp. 220-228, 1998.

[31] L. Li and A. A. Sagüés, "Chloride Corrosion Threshold of Reinforcing Steel in Alkaline Solutions - Open-circuit Immersion Tests", *Corrosion,* vol. 57, 2001.

[32] A. A. Sagüés "Implementation of SHRP Corrosion Diagnosis Projects in Planning Maintenance Strategies for Florida Bridges", Final Report WPI 0510862, Florida Department of Transportation Research Center, Tallahassee, FL., 2002.

[33] A. A. Sagüés, "Modeling the Effects of Corrosion on the Lifetime of Extended Reinforced Concrete Structures", *Corrosion,* vol. 59, pp. 854-866, 2003.

[34] H. Kaesche, *Metallic Corrosion*. NACE International, Houston, TX., 1996.

[35] A. N. Sánchez and A. A. Sagüés, "Potential-Dependent Chloride Threshold in Reinforced Concrete Damage Prediction – Effect of Activation Zone Size". Paper No. 2704 presented at the NACE Corrosion 2013, Orlando, FL. NACE International, Houston, TX., 2013.

[36] A. A. Sagüés, A. N. Sánchez, K. Lau, and S. C. Kranc, "Service Life Forecasting for Reinforced Concrete Incorporating Potential-Dependent Chloride Threshold", *Corrosion In Press,* 2014.

[37] A. N. Sánchez and A. A. Sagüés, "Probabilistic Corrosion Forecasting of Steel in Concrete with Potential-dependent Chloride Threshold". Procedings of the 1st International Conference on Ageing of Materials & Structures. Editors: K. van Breugel and E.A.B Koenders. Delft University of Technology. Delft, The Netherlands, 2014.

[38] A. A. Sagüés, S. C. Kranc, and F. J. Presuel-Moreno, "Applied Modeling for Corrosion protection Design for Marine Bridge Substructures", Final Report Contract No. B-9119, Florida Department of Transportation Research Center, Tallahassee, FL.,1997.

[39] A. A. Sagüés, S. C. Kranc, F. Presuel-Moreno, D. Rey, and A. T.-A. L. Yao, "Corrosion Forecasting for 75-Year Durability Design of Reinforced Concrete", Final Report Contract No. BA502, Florida Department of Transportation Research Center, Tallahassee, FL., 2001.

[40] P. B. Bamforth, “The Derivation of Input Data for Modelling Chloride Ingress from Eight-Year UK Coastal Exposure Trials”, *Magazine of Concrete Research*. pp. 87-96, 1999

[41] A. A. Sagüés, J. Lee, X. Chang, H. Pickering, E. Nystrom, W. Carpenter, S. C. Kranc, T. Simmons, B. Boucher, and S. Hierholzer, "Corrosion of Epoxy Coated Rebar in Florida Bridges", Final Report Contract No. 0510603, Florida Department of Transportation Research Center, Tallahassee, FL., 1994.

[42] P. Mangat and B. Molloy, "Prediction of Long Term Chloride Concentration in Concrete", *Materials and Structures,* vol. 27, pp. 338-346, 1994.

[43] NORDTEST NT BUILD 492: “Concrete, Mortar and Cement-Based Repair Materials: Chloride Migration Coefficient from Non-Steady-State Migration Experiments", P.O. Box 116 FIN–02151, Espoo, Finland, 1999.

[44] F. J. Presuel-Moreno,"Analysis and Estimation of Service Life of Corrosion Prevention Materials Using Diffusion, Resistivity, and Accelerated Curing for New Bridge Structures", Final Report Contract No. BDK79-977-02, Florida Department of Transportation Research Center, Tallahassee, FL., 2013.

[45] M. F. Hurley and J. R. Scully, "Threshold Chloride Concentrations of Selected Corrosion-Resistant Rebar Materials Compared to Carbon Steel”, *Corrosion,* vol. 62, pp. 892-904, 2006.

[46] P. F. Marques, A. Costa, and F. Lanata, "Service Life of RC Structures: Chloride Induced Corrosion: Prescriptive Versus Performance-Based Methodologies", *Materials and Structures,* vol. 45, pp. 277-296, 2012.

APPENDIX 1

Reinforced Concrete Durability Model Prototype – Users Guide

Alpha Version A1.1 June 2014

Program version not for public release. Subject to corrections and updates. The purpose of this version is to establish functionality with no representation of accuracy of the parameters used or of the output. Application is contingent on updated adoption of an appropriate set of parameter values and simplifying assumptions. See main body of Final Report for further qualifications.

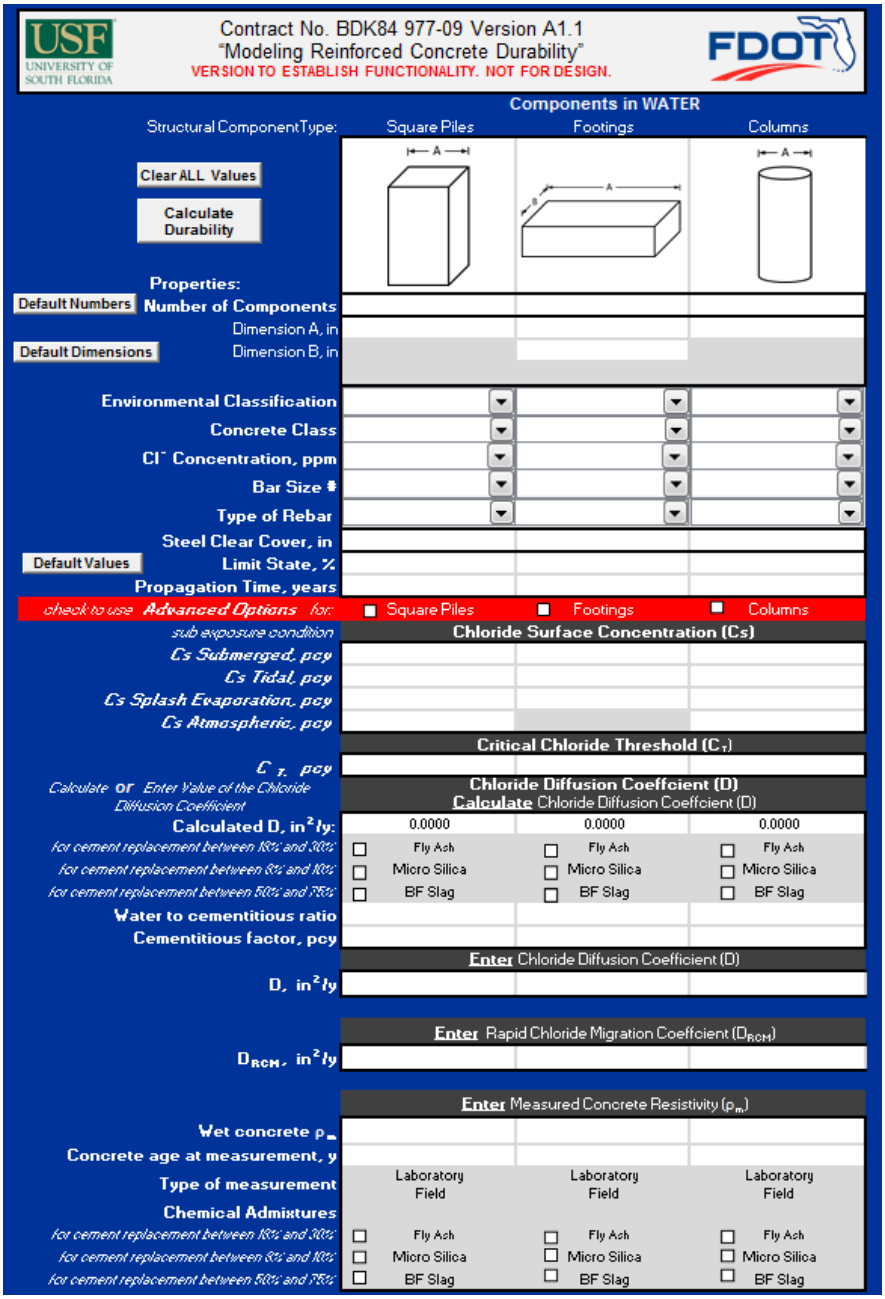

Prepared by: Andrea N. Sánchez and Alberto A. Sagüés

General Description. For a Step-by-Step tutorial proceed to Page 64.

The User Interface for the "Reinforced Concrete Durability Model Version A1.1" is shown in Figure A 1, in the following program description, it is assumed that the user has only access to the "Components in Water", "Components in Soil" and "Results" tabs.

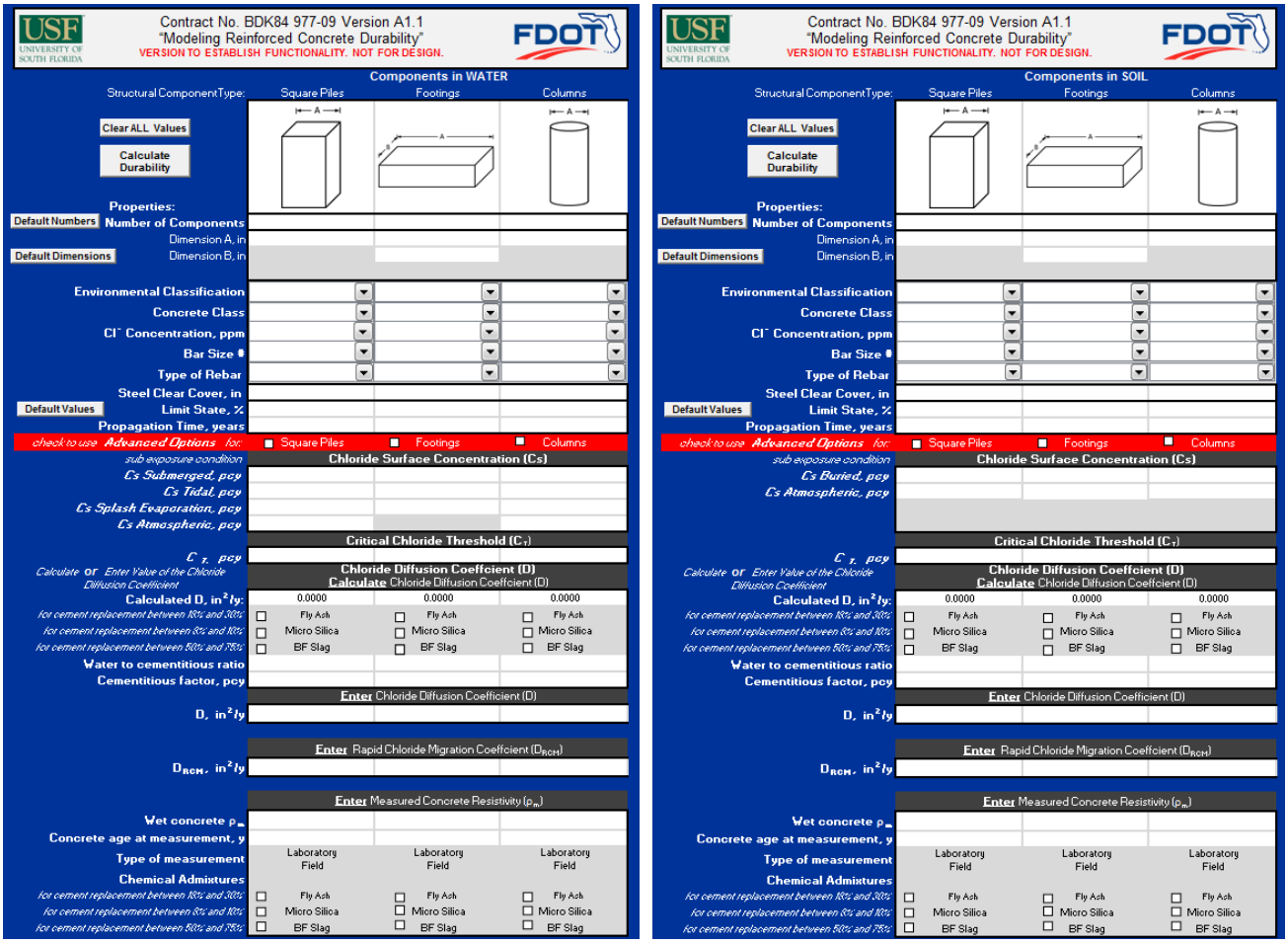

Figure A 1 User interface

The program has three worksheet tabs available for the user, these are:

- Components in Water
- Components in Soil
- Results

The "Components in Water" and "Components in Soil" tabs correspond to the data entry user interface. Both tabs contain very similar information, therefore, the description of the main and advanced input features of the data entry tabs will be based on "Components in Water" tabs, and is given in the following section.

User interface

The program allows the user to evaluate the durability of various structural components by specifying the dimensions, the exposure aggressiveness, the concrete quality, the steel bar material type and size used, among others. Below is a description of the data entry parts of the model. Version A1.1 includes both Basic and Advanced Calculation Options that are described subsequently.

Structural Component type:

Three structural component types were implemented in the program to evaluate the durability: Square Piles, Rectangular Footing and Round Columns in Water and in Soil. Durability calculation can be performed separately (e.g., calculate durability of Square Piles only) or as a group.

Number of components in water and number of components in soil:

The user introduces the number of structural component type category in a given bridge category for a given exposure type (water and/or soil). If the user does not intend to evaluate the durability of a structural component type or an exposure type, the corresponding cells should be left as a blank or with the number zero (0).

A “Default Numbers” bottom is located on the left-hand side of the “Number of Components” label. By clicking the bottom, default values for the structural components type will appear.

Dimensions:

The dimensions for each structural component type are introduced by the user in accordance to the denoted letter shown in the corresponding figure.

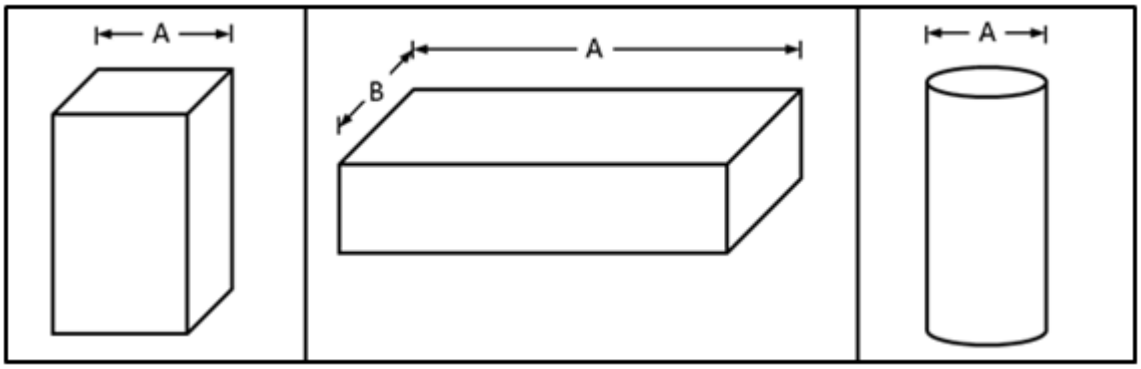

Figure A 2 Geometry of the structural components

A “Default Dimensions” bottom is located on the left-hand side of the “Dimension A, in”, “Dimension B, in”, in” labels in the worksheet. By clicking the bottom, default dimension values for the components will appear. Note: the current alpha model version A1.1 assumes that the components in water and the component in soil have equal dimensions.

Environmental Classification:

This fragment of the data entry is part of the Basic Calculation Options. The user can select from the three specified environmental classifications in accordance to the FDOT Structural Design Guidelines (SDG): Extremely Aggressive, Moderately Aggressive and Slightly Aggressive, in the order of high corrosion risk to low corrosion risk as shown in Figure A 3.

The program allows the user to select one environmental classification per component in water and component in soil. When the user selects a environmental classification for a given component for a given exposure type, a message box appears on the screen asking if the user wants to use the prescriptive values designated in the SDG for the concentration of chlorides at the surface of the concrete and the steel clear cover for the given exposure type (in water or in soil). If the answer is yes, then values for those parameters will appear in the corresponding cells as shown in the Figure A 4 for the case of a Square Pile with components in water. If the answer is no, the user has to select/enter their own preferred values for the Cl^- concentration and steel clear values, which is explained in much detail later on.

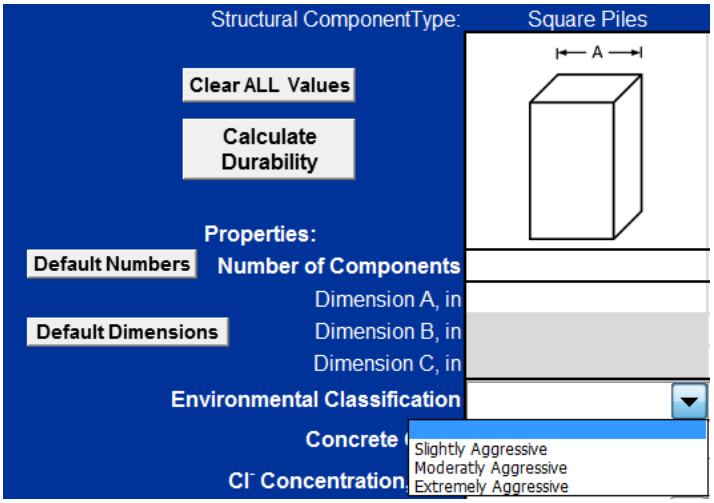

Figure A 3 Environmental classification for Square Piles

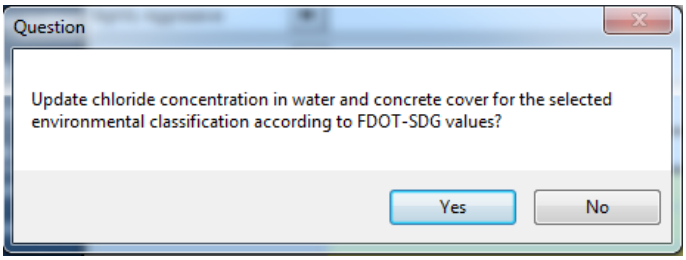

Figure A 4 Message box to update chloride concentration and concrete cover values in accordandce with FDOT-SDG

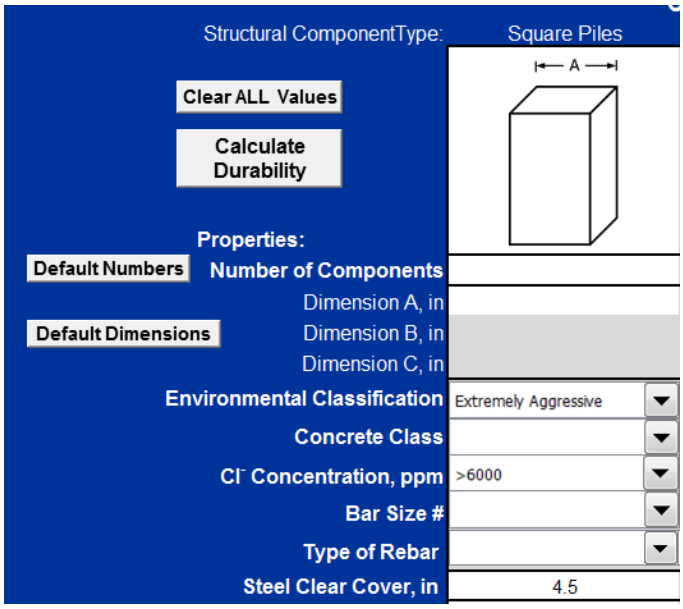

Figure A 5 Default values (highlighted) in accordance to the FDOT-SDG

Concrete Class:

Six FDOT concrete Classes (I though VI) can be selected by the user as shown in Figure A 6. A nominal preselected chloride diffusion coefficient is assigned for each concrete class as explained for Table 5 in the main body of the report. User-selected alternative diffusion coefficient values can be entered overriding the preselected values.

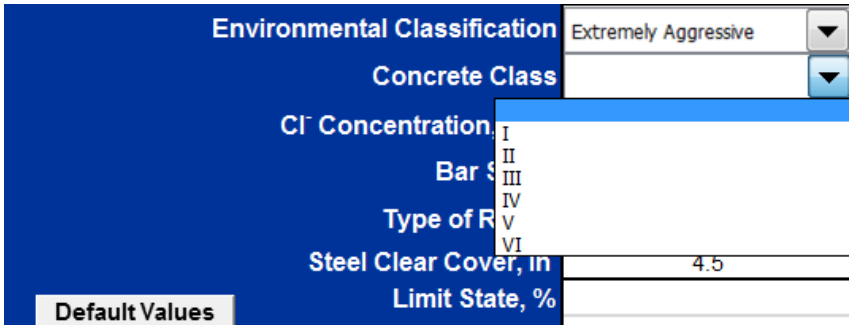

Figure A 6 Range of concrete classes

Chloride concentration:

The user can select two options for the chloride concentration in the body of water and soil: ≤6000 ppm and >6000 ppm. As specified by the SDG, the former value corresponds to a Slightly and a Moderately Aggressive Environment, and the latter value to the Extremely Aggressive, respectively as exemplified in Figure A 7.

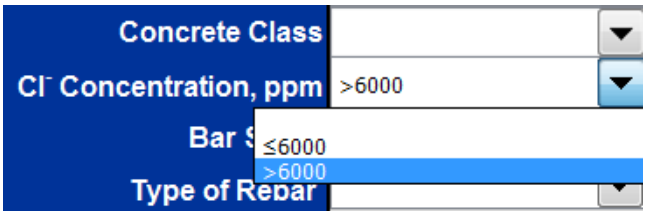

Figure A 7 Options for the Chloride concentrntration in water

When the user selects the environmental Cl^- concentration for a given structural component, by default the program assigns the C_S values for each sub-exposure type per Table 5 in the main body of the report. Alternatively, user-selected Values of C_S for each sub-exposure can be entered by clicking on the advanced user check box, as explained in the "Advanced Options" section.

Bar size and type of rebar:

Selections of steel bar sizes and rebar material type are available for input as shown in Figure A 8. A correction factor to obtain a fictitious increased diffusion coefficient is obtained through the rebar diameter Φ_r and cover value. The type of rebar specifies the value of the nominal base corrosion threshold C_T per Table 5 in the main body of the report. The value of C_T can be alternatively specified by the user as indicated in the "Advanced Options" section.

Figure A 8 Bar size options and type of rebars incorporated in the program

Limit State and Time of Propagation:

A limit state default value of 2.3% (as an example, not intended at present as a recommendation) appears as a nominal selection for the three structural component types when the “Default Values” is clicked in the “Components in Water” and “Components in Soil” tab. Also, that 2.3% value is set as default value for limit state of the whole bridge, which can be also modified in the “Results” tab. Alternatively, the user can enter any desired limit state value, to aid in interpretation when the results are presented as a global damage function, or as a damage function for a given type of structural component/service combination.

A Propagation Time of 5 years is also entered when the “Default Values” box is clicked. Alternatively, the user can assign any desired value to account for the propagation stage duration.

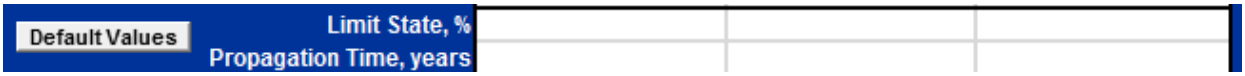

Figure A 9 Limit State and Propagation Time

Advanced options:

The user can modify the values for the chloride surface concentration, chloride threshold, and diffusion coefficient by clicking on the advanced options for a given element.

User-selected chloride surface concentration values can be inserted for each sub-exposure condition. For example, if user clicks on the Advanced Options check mark for Square Piles in Water and enters the preferred C_S values for each given sub-exposure conditions (Cs submerged, Cs Tidal, Cs splash Evaporation and Cs atmospheric) as shown in Figure A 10, then the C_S values given in Table 5 of the main body of the report for the Extremely Aggressive condition (as selected and shown in Figure A 10) are disregarded by the program and replaced by those values entered by the user. However, if for example the user only enters a C_S value for the C_S Atmospheric sub-exposure zone while leaving the other entries blank, then the program will still use the default C_S values, in accordance to the Environmental Classification selected, for the remainder sub-exposures (C_S Submerged, C_S Tidal and C_S Splash Evaporation).

User-selected values of C_T can also be entered for each structural component and exposure condition (water and soil). However, the user can still choose to retain the default values in any category by leaving the corresponding cell/cells blank, as long as the rebar material type and concrete class was indicated in the basic options.

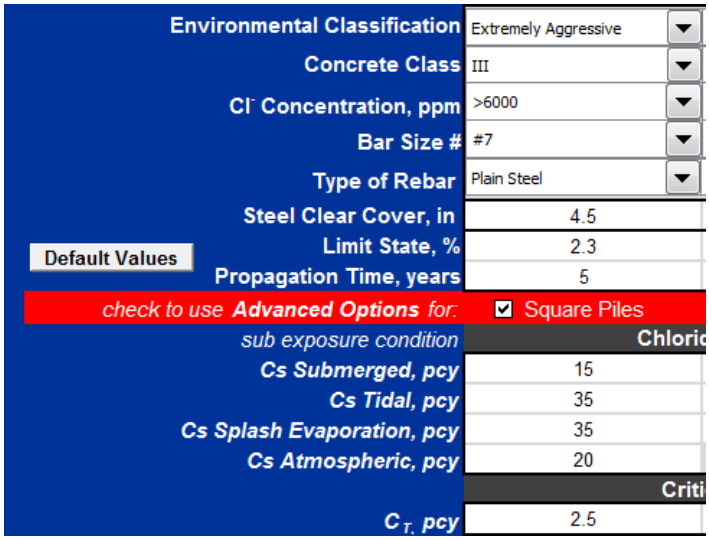

Figure A 10 Example of Advanced options

A user-selected value of the chloride diffusion coefficient can be entered directly under the "Enter Chloride Diffusion Coefficient (D)" label. Similarly as the C_S and C_T user entries, if cells for entering the value of D are left blank, then the program uses the default values assigned through the information provided for the concrete class.

Alternatively, the user can have the program make an estimate of the diffusion coefficient by specifying the water-to-cementitious ratio w/ct, the percentage of cement replacement by chemical admixtures (Fly Ash, Micro Silica, and BF Slag) within the limits indicated in the form, if applicable, and the cementitious factor CF. The resulting value will appear under the "Calculate Chloride Diffusion Coefficient (D)" label. As indicated in the main body of the report, this estimate is more appropriate for the higher concrete classes, as the calculation estimate is limited to 0.33< w/ct < 0.41, and 650 pcy < CF < 748 pcy.

Placeholder features to admit user input to obtain the chloride diffusion coefficient value through a) experimental results of the Nordtest NT BUILD 492 test (rapid chloride migration), and b) through the concrete resistivity and permeability data ware included in the model entry form as shown in Figure A 11. However, the functionality of these features is not supported at present and is pending on future work.

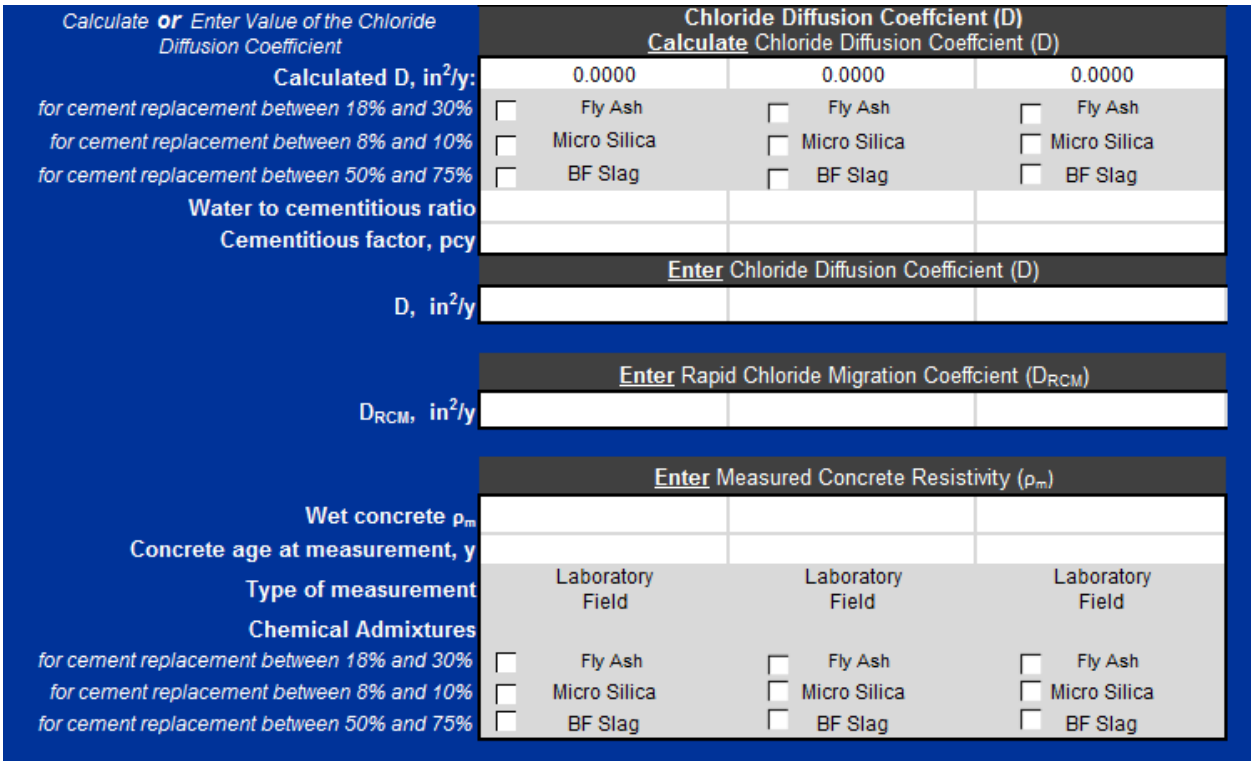

Figure A 11 Advanced options for chloride diffusion coefficient

Output:

Results are shown under the “Results” tab. Every graph has a black dashed vertical line that indicates a nominal 75-year service life. The limit states entered in the data entry worksheets were specific for each type of structural component, but the first set of plots located on the left-hand side show the weighted result of all the conditions and exposure analyzed. For this type of evaluation (to be interpreted at the user’s discretion), a global limit state can be entered by the user in cell “B8” for the left-hand graphs if it is desired to override the nominal default value of 2.3%. As noted earlier, the significance and application of the limit state concept is subject to user interpretation and the default values are not intended as a recommendation.

The top-left graph represents the damage function of the bridge as a whole; it includes the concrete surface cumulative damage (in linear scale) of all the structural components in water and in soil that were evaluated. The middle-left plot indicates in a logarithmic scale the concrete surface cumulative damage for the entire bridge as well as for each structural type, regardless of the exposure condition (water or soil). For example, the curve labeled Footings indicates the percentage of the surface of all the Footings that has reached the damage condition for a given age. The log scale was used to facilitate reading of results that may span a wide range of values. For ease of comparison to the top graph, the bottom left plot shows the same results as the one in the center but the damage is in linear scale.

The second set of plots placed on the right-hand side from top to bottom correspond to the concrete surface cumulative damage for the Square Piles, Footings and Columns,

respectively, for each exposure condition (in water and in soil). Limit state lines in those graphs reflect either the default value or the alternative values that were provided by the user in the entry forms.

It is emphasized that these displays are representative, but not limiting, examples of user experience. Since the model calculates the specific damage function for each of the component/exposure Classes evaluated, alternative displays geared to specific user needs can be easily added in custom versions of the program through the ordinary graphic options in the spreadsheet. For example, a custom graph can be quickly created to display the damage progression of 2-way corners of square piles in the splash-evaporation sub-exposure regime for components in water, when specific design decisions are to be made for that combination.

Step-by-Step Tutorial – *Basic Options:*

This Step-by-step tutorial exemplifies application to a hypothetical bridge with nominal default numbers of square piles, footings and columns in water and in soil. Only entries in the "Components in Water" and "Components in Soil" are to be made. Altering any other tab will compromise program operation. This program has been tested with Excel 2010; Excel needs to be installed in the computer and appropriate options enabled.

Program instructions:

1. Open the file "Alpha A1.1 BDK84 977-09". (Enable Macros if asked).
2. In the excel spreadsheet select the tab "Components in Water"
3. Click the "Clear All Values" button located on the top-left, above the "Calculate Durability" button.
4. Click the "Default Numbers", "Default Dimensions" and "Default Values" buttons (located at the far left-hand side of the spreadsheet) to populate the hypothetical bridge parameters with a nominal population of structure components of given dimensions, exposure conditions, and propagation time and limit state. Any of those values can be changed at will by the user by entering the chosen amount in the corresponding cell.
5. Click on the dropdown box (inverted triangle) on the left side of the "Environmental Classification" label for Square Piles and select "Extremely Aggressive". A message box will appear asking if to "Update chloride concentration in water and concrete cover for the selected environmental classification according to the FDOT-SDG values?" Click on "Yes". Automatically ">6000" will appear in the dropdown box for the Chloride Concentration in Water and a value of "4.5" will show in the Steel Clear Cover of Components in Water.
6. Repeat step 5 to select the environmental classification for the Footings and Columns.
7. Click on the dropdown box for the "Concrete Class" for Square Piles and select "IV", for Footings select "IV", and for the Columns select "IV".
8. Click on the dropdown box for the "Bar Size" for Square Piles and select "#6", for Footings select "#7", and for Columns select "#4".
9. Click on the dropdown box for the "Type of Rebar" and select "Plain Steel" for Square Piles, Footings and Columns.
10. The "Components in Water" sheet should have the same values and conditions as in Figure A 12. If yes, proceed to step 11. If not, make changes accordingly.
11. In the excel spreadsheet select the tab "Components in Soil"
12. Repeat steps 3 to 9.
13. The "Components in Soil" sheet should have the same values and conditions as in Figure A 12 shown below. If yes, proceed to step 14. If not, make changes accordingly.
14. Click on "Calculate Durability" button in either the "Components in Water" tab or in "Components in Soil" sheet. The entire worksheet will be calculated in either case.

Only one of the “Calculate Durability” buttons needs to be clicked. Results will appear after a brief wait.

15. Results are shown in the “Results” tab and should be similar to those shown in Figure A 13. The limit state for the whole bridge is entered in cell “B8”. The example shown in Figure A 13 has a Bridge limit state value set to 2.3% (for demonstration purposes only), but the user can modify the limit state value without altering the cumulative damage results obtained. In this tutorial example, conditions were chosen so as to project an appreciable amount of damage before 75 years for visual clarity only and not as a design recommendation. Likewise, the limit state values used for the bridge and structural components are placeholder values to illustrate graphic display and not intended as a technical recommendation.

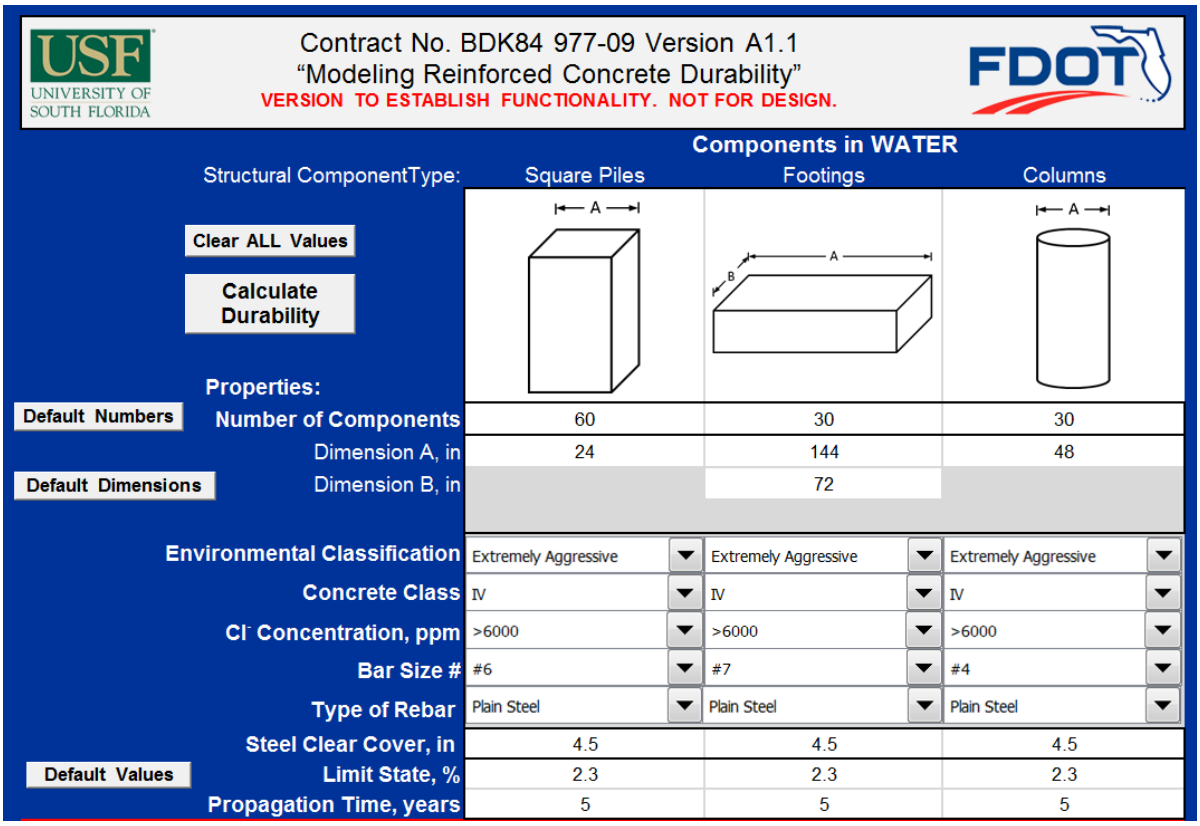

Figure A 12 Screen shot of “Components in Water” tab with the tutorial input information before step 14

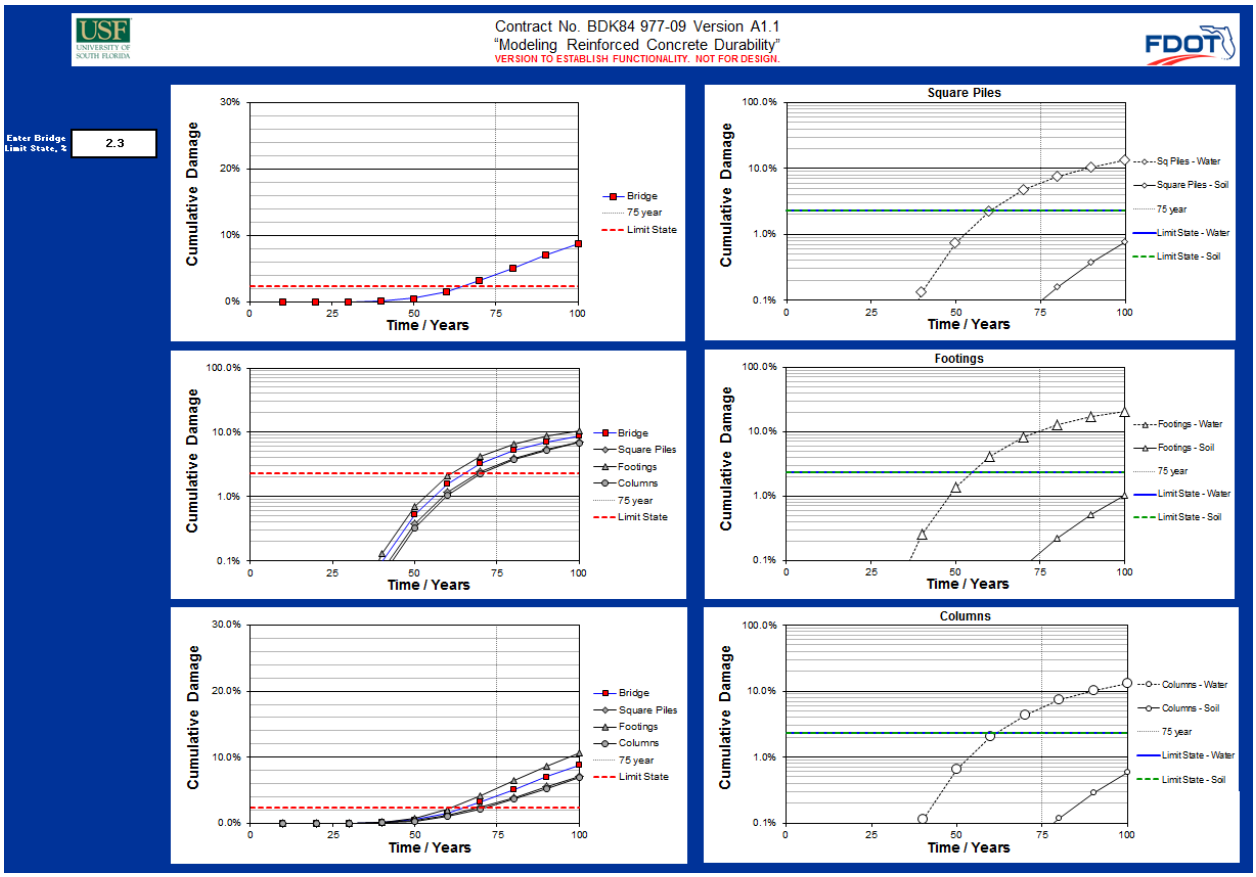

Figure A 13 Results of the example given in Step-by-Step tutorial